An electrically coupled pioneer circuit enables motor development via proprioceptive feedback in *Drosophila* embryos

Xiangsunze Zeng,[1] Yuko, Komanome,[1] Tappei Kawasaki,[1] Kengo Inada,[2] Julius Jonaitis,[5] Stefan R. Pulver,[5] Hokto Kazama,[2,4*] and Akinao Nose[1,3,6*]

[1]Graduate School of Frontier Sciences, The University of Tokyo, 5-1-5 Kashiwanoha, Kashiwa, Chiba 277-8561, Japan

[2]RIKEN Center for Brain Science, 2-1 Hirosawa, Wako, Saitama 351-0198, Japan

[3]Graduate School of Science, The University of Tokyo, 7-3-1 Hongo, Bunkyo-ku, Tokyo 113-0033, Japan

[4]Graduate School of Arts and Sciences, The University of Tokyo, 3-8-1 Komaba, Meguro-ku, Tokyo 153-8902, Japan

[5]School of Psychology and Neuroscience, University of St Andrews, St Mary's Quad, South Street, St Andrews KY16 9JP, UK

[6]Lead Contact

*Correspondence: hokto.kazama@riken.jp (H.K.), nose@k.u-tokyo.ac.jp (A.N.)

SUMMARY

Precocious movements are widely seen in embryos of various animal species. Whether such movements via proprioceptive feedback play instructive roles in motor development or are mere reflection of activities in immature motor circuits is a long-standing question. Here we image the emerging motor activities in *Drosophila* embryos that lack proprioceptive feedback, and show

that proprioceptive experience is essential for the development of locomotor central pattern generators (CPGs). Downstream of proprioceptive inputs, we identify a pioneer premotor circuit composed of two pairs of segmental interneurons, whose gap-junctional transmission requires proprioceptive experience and plays a crucial role in CPG formation. The circuit autonomously generates rhythmic plateau potentials via IP_3-mediated Ca^{2+} release from internal stores, which contribute to muscle contractions and hence produce proprioceptive feedback. Our findings demonstrate the importance of self-generated movements in instructing motor development, and identify the cells, circuit, and physiology at the core of this proprioceptive feedback.

INTRODUCTION

Animals start to move while in the womb or egg[1,2]. For instance, a human fetus makes an array of movements such as wiggling, kicking and sucking in mother's womb. Similarly, *Drosophila* embryos start to twitch and crawl in the egg shell. These precocious movements are initially local and uncoordinated but are later replaced by more sophisticated behaviors similar to those seen after birth or hatching[3,4]. In many animal species, early movements are intrinsically generated by spontaneous activities in a small number of cells in the spinal cord[5–9]. These spontaneous activities are often seen to propagate in electrically coupled circuits and are thought to guide the formation of larger circuit(s) generating more sophisticated movements[8–15]. However, how these spontaneous activities emerge, organize patterned activities and finally contribute to the formation of functional central pattern generating (CPG) circuits remain poorly understood[1,2] despite a long-standing investigation[3,8,9,16–18].

Muscular contractions induced by spontaneous motor activities in turn activate the proprioceptive system which sends information back to the central nervous system (CNS)[19–20]. It has long been hypothesized that precocious movements and ensuing proprioceptive feedback represent a trial-and-error process that allows the developing central circuits to gauge the effectiveness of movements and adaptively shape themselves in an experience-dependent manner[2,21–23]. However, due to the difficulties in specifically manipulating neural activities during development, whether and how proprioceptive experience regulates the development of motor circuits still remain elusive.

The *Drosophila* embryonic/larval CNS provides an attractive opportunity to address this issue. In this numerically tractable system, connectomics analyses (3D reconstruction of electron microscopy images)[24] identified neural circuits that regulate peristaltic locomotion, a major behavior of the larvae generated by rhythmic waves of muscular contractions propagating along the anterior-posterior axis of the body[25–28]. Furthermore, highly sophisticated gene manipulation methods allow functional analyses at single-cell resolution[29,30]. Capitalizing on these advantages, here we study the embryonic development of central circuits that generate larval locomotion and directly assess the impact of specific deprivation of proprioceptive feedback on CPG development with calcium imaging. We find that the locomotor CPGs fail to form in the absence of proprioceptive experience. Proprioceptive input acts on gap-junctional connections in an intersegmental circuit comprising two pairs of segmental interneurons, A27h and M, which are found to be essential for CPG development. The circuit is intrinsically active from the earliest stage of motor development via inositol 1,4,5,-trisphosphate receptor (IP_3)-mediated release of calcium from the internal stores, and induces precocious muscular contractions. Therefore, the pioneer circuit

senses the feedback of its outputs and enables development of the entire locomotor network. Our findings not only provide experimental evidence for a crucial role played by proprioceptive feedback in the development of motor circuits, but also show how a pioneer circuit enables activity-dependent development of a locomotor network.

RESULTS

Proprioceptive experience is required for the proper development of locomotor CPGs

The motor behavior of *Drosophila* embryos develops in a gradual manner, from single-segment twitches, to simultaneous contractions of muscles in several segments, and eventually to peristalsis consisting of sequential contraction of bilateral muscles throughout the body[3,4]. As in other animals, proprioceptive feedback is important in regulating moment-to-moment locomotion in the larvae[31,32]. To distinguish the role of proprioception in development from that in locomotion, we used pan-neuronal calcium imaging in the isolated CNS to study the formation of fictive locomotion, which reflects the activity of CPGs in the absence of sensory feedback[33–35] (Figure 1A). In line with the observation of muscular movements[3], the CPG activities developed progressively from initial sporadic and local activities (hereafter called “sporadic”), to intersegmentally synchronized activities (“synchronized”), and finally to wave-like propagation throughout the nerve cord in a forward or backward direction (“complete waves”) in wild-type embryos (Figures 1B and 1D).

Three types of sensory neurons, Class I dendritic arborization (da), bipolar dendrite (bd) and chordotonal neurons, have been implicated in proprioception required for smooth locomotion in the larvae[31,32,36–38]. Because these neurons innervate the CNS prior to the emergence of motor activities[39] (Figures S1A–S1D), they are likely to

mediate proprioception from the beginning of motor development. To study the role of proprioception in this process, we used a mutation of NOMPC (No mechanoreceptor potential C), a mechanotransduction channel expressed in these cells[37]. In *nompC*$^{1/3}$ trans-heterozygous embryos, initial sporadic activities occurred normally. However, synchronized and wave-like CPG activities did not appear during embryogenesis and the first instar larval stage (Figures 1C and 1D), strongly suggesting that proprioceptive experience prior to the appearance of synchronized activities (~17 h AEL) is critical for the formation of patterned CPG activities. To further confirm the importance of proprioceptive experience in CPG development, we also examined loss-of-function mutations of two other genes: *mhc* (myosin heavy chain), which encodes the motor protein essential for muscle contraction[40] and *GluRIIC,* which encodes a subunit of the muscle glutamate receptor essential for neuromuscular transmission[41]. *Mhc*^{1} homozygotes generate no muscular contraction[40], thus no proprioceptive feedback. In *GluRIIC* homozygotes, neurally-driven muscle contractions are compromised[3]; hence the accompanying proprioceptive feedback should also be absent in these mutants. Note, however, autonomous muscle contractions that occur independent of neural control remain in *GluRIIC* mutants[3]. We found that complete waves entirely fail to form in *Mhc*^{1} and *GluRIIC* mutants (Figure S1E) as in *nompC*$^{1/3}$ mutants. These results provide strong evidence that proprioception is required for the proper development of functional CPGs. We also studied synchronized activities and found that they were also absent in *Mhc*^{1} embryos (Figure S1F). However, these activities occurred in *GluRIIC* mutants albeit less frequently (Figure S1F), suggesting that proprioception of autonomous muscle contractions could play some roles in the formation of synchronized activities.

A gap-Junctionally coupled circuit generates synchronized activity during early motor development

How might proprioception regulate the development of CPG circuits? We focused on the segmentally repeated premotor interneurons A27h as a candidate target of proprioceptive feedback because these neurons are thought to be key elements of a CPG circuit driving forward locomotion and receive direct input from proprioceptors[25] (Figure 2A). We used *R36G02-Gal4*[25] to specifically label and/or manipulate A27h and its putative sibling neuron termed M (Figures 2B–2E and S2A). Although fortuitously identified because of its shared *Gal4* expression, M neuron together with A27h was found to have crucial functions in motor development as described below. Cell-type specific imaging in *R36G02-Gal4 > UAS-GCaMP6m* embryos revealed that both cells started to exhibit local calcium transients at ~16 h after egg laying (AEL; Figures S2B and S2C), the time sporadic activities were first observed in pan-neuronal imaging (Figure 1). Shortly after, intersegmentally synchronized activities occurred and eventually, complete waves emerged at ~18.5 h in these cells (Figures S2B and S2C). The early activity onset of M and A27h neurons suggests that they are among the first to be recruited to the CPG circuits. We closely studied the intersegmentally synchronized events and found that coactivations not only occurred within the same cell type (i.e. among A27h or M neurons in different segments; Figures S2B and S2C), but also across the two cell types (Figures 2F and 2G). The strength of synchronization progressively increased during development (Figures 2F and 2G).

Neuronal synchronization suggests the existence of electrical coupling[42–44]. Indeed, application of a potent gap junction blocker, carbenoxolone (CBX) abolished synchronized and wave-like activities in A27h and M neurons (Figures 3A and 3B). Furthermore, A27h and M neurons in neighboring neuromeres were found to be dye-

coupled (hereafter called cognate coupling). The dye injected into M neurons diffused frequently to M neuron in the next anterior neuromere and occasionally to A27h neurons in the same and/or neighboring neuromeres (Figures 2H and 2I). In contrast, cognate coupling was never seen from M neurons to posterior cognates or when the dye was injected to A27h neurons (Figure 2J, left), suggesting that these cells are connected through rectifying gap junctions[45]. We also noted segmental-specificity: cognate-coupling was only seen in anterior neuromeres (from T3 to A3; Figure 2J, right). Such anterior-posterior heterogeneity in electrical coupling and/or cellular synchronization has also been reported in the spinal cords of zebrafish and mice[8,15]. Altogether, the above data indicate that M and A27h neurons are electrically coupled to form an intersegmental circuit and generate synchronized activity in the nascent motor network (Figure 2K). Finally, A27h and M neurons were also coupled to other interneurons in the nerve cord (6±1.2 cells (n = 25) for M and 8±1.0 cells (n = 17) for A27h neurons, non-cognate coupling, Figure S3). Thus, developing circuits in *Drosophila* embryos are gap-junctionally coupled.

Electrical but not chemical transmission in the M/A27h circuit is essential for motor development

The early synchronization in the M/A27h circuit implies that electrical transmission in the circuit takes a pioneering role in motor development. To test this, we examined the effects of cell-type-specific knockdown of gap junctional proteins (encoded by *innexins*) on larval locomotion. When ShakB, Ogre or Innexin5 but not the other Innexins in *Drosophila* were knocked-down in A27h and M neurons, the stride duration of larval locomotion was significantly prolonged (Figures 3C and S4C). In contrast, disruption of chemical transmission from M and A27h neurons by expression of

tetanus toxin light chain (TeTxLC) did not perturb peristaltic locomotion in newly hatched larvae (Figures S4A and S4B). These results suggest that electrical but not chemical transmission in these cells is important for the development of locomotor circuit.

To further examine the role of M/A27h electrical connections, we studied the effect of Innexin knock-down on the development of patterned motor activity during embryogenesis by expressing GCaMP in these cells. Knockdown of ShakB greatly decreased the strength of synchronized activities among A27h and M neurons (Figure 3A), and disrupted both cognate and non-cognate coupling in the M/A27h circuit irrespective of injected segments or developmental stages (Figures 3D and 3E). Furthermore, complete waves failed to be generated in the circuit (Figure 3B). Thus, gap-junctional transmission mediated by ShakB is essential for the formation of patterned activities in the M/A27h circuit. In contrast, no such dramatic effects were observed by knockdown of Ogre or Innexin5 (Figures S4D and S4E). This may be because knockdown of these innexins impairs gap-junctional connections between the M/A27h circuit and other CPG components, which are crucial for functional CPG development but are dispensable for that of the M/A27h circuit itself.

We also generated a split-Gal4 line that selectively targets M neurons (*M-split-Gal4*; Figure S4F) to test if disrupting ShakB solely in M neurons impairs motor development. We found that knockdown of ShakB in M neurons greatly prolonged the stride duration (Figure 3C), indicating essential roles played by them. Because we could not generate A27h-specific Gal4 lines, whether A27h neurons are similarly pivotal remains to be determined.

Cognate coupling is specifically abolished in the absence of proprioceptive experience

The results thus far show that perturbation of proprioception and its putative target M/A27h circuit both disrupt motor development from an early phase when synchronized activities appear. This raises a possibility that proprioception controls motor development in part by regulating electrical transmission in the M/A27h circuit. To test this, we examined dye-coupling in *nompC*$^{1/3}$ mutants and indeed found that cognate coupling in the M/A27h circuit normally seen in anterior neuromeres (T3-A3) was completely abolished (Figure 4). In contrast, the number of non-cognate coupling remained comparable to wild type throughout embryonic development (Figure 4B). These results show an essential role of proprioception in maturation of electrical transmission that is exerted with high specificity in the M/A27h circuit.

Chemical synaptic input to and spiking output from A27h neurons are impaired in the absence of electrical coupling or proprioception

In many animal species, initially electrically coupled circuits later become chemically-driven[12,13,46], suggesting that electrical synapses regulate chemical signaling during development. We therefore tested whether chemical signaling is also affected in ShakB-knockdown mutants. We performed whole-cell patch-clamp recording to assess spontaneous excitatory postsynaptic potentials/currents (EPSPs/EPSCs) along with other physiological properties in A27h and M neurons (Figures 5A–5C and S5). In wild type A27h neurons, EPSPs increased in number over time (Figure 5B). These EPSPs are mediated largely by nicotinic acetylcholine receptors, since they were virtually abolished by bath application of mecamylamine but not atropine (Figure 5C). When ShakB was specifically knocked down in A27h and M cells, synaptic inputs

retained their amplitude but became infrequent throughout development (Figures 5A–5C and S5E), suggesting that decreased electrical coupling in the M/A27h circuit reduces excitatory chemical inputs to A27h neurons. We also observed less abundant EPSPs in A27h neurons in *nompC*$^{1/3}$ mutants (Figures 5A–5C), consistent with the loss of dye coupling among M and A27h neurons in the mutants (Figure 4). We further found the resting membrane potential and spontaneous firing rate to be markedly reduced in ShakB-knockdown or *nompC*$^{1/3}$ mutants (Figure 5D). These results suggest that electrical transmission in the M/A27h circuit is required for properly receiving chemical input and delivering spiking output in A27h neurons.

M neurons periodically produce plateau potentials via release of calcium from internal stores during early motor development

Although the above data demonstrate the crucial function of proprioceptive feedback in the development of motor circuit, the source of activity that drives precocious movements in the first place still remained elusive. Since M/A27h circuit is active from an early developmental phase (Figures S2B and S2C) and A27h neurons can activate motor neurons[25] (Figure 2A), the circuit may also be involved in generating initial muscular movements. We therefore pursued this possibility and found it to be the case.

Electrophysiological experiments showed that M neurons spontaneously ($I_{command}$ = 0 pA) exhibited plateau potentials[47,48] from early developmental stages which eventually became periodic and accompanied burst firing (Figures 6A–6D). In 19-24 h, plateau potentials were seen in all M cells examined (n = 52 cells) at an average frequency of ~6/min (Figure 6G, Control). Although similar burst firing was also seen in 9 out of 54 A27h neurons, these activities were abolished by CBX (Figures S6A and S6B), suggesting that they originated in M neurons and spread to A27h neurons

through gap junctions. To examine if plateau potentials are commonly seen in other neurons, we performed current-clamp recordings from 86 randomly selected cells in the nerve cord (Figures S7A–S7E). Plateau potentials were only seen in 4 out of the 86 cells (Figures S6B and S6C), suggesting that they are rare in embryonic central neurons if not unique to M cells. Principle component analysis (PCA) of activity features (Figures S6D–S6G) of all recorded cells revealed that M neurons were separated from A27h and randomly selected neurons, which was quantified by a nonlinear support vector machine (SVM) classifier (Figure 6E). This indicates that the activity pattern of M neurons is distinct from A27h and other cell types.

We next asked whether M neurons generate plateau potentials intrinsically or in response to inputs from other cells. Unlike A27h neurons, M neurons rarely received EPSPs throughout development (Figures 5B and 5C). Moreover, plateau potentials persisted in the presence of channel antagonists that inhibit chemical ($CdCl_2$ or TTX) or electrical transmission (CBX), or when proprioception was inhibited (*nompC*$^{1/3}$; Figures 6F and 6G). These results suggest that the plateau potentials are generated autonomously in M neurons.

To examine how plateau potentials are generated in M neurons, we first investigated the possible involvement of canonical pacemaker currents. However, this hypothesis was rejected as plateau potentials were not blocked by antagonists of I_h, I_{Na} and I_{Ca}[49,50] (Figures 6F and 6G). We therefore turned to internal calcium release from endoplasmic reticulum[51] that can depolarize the membrane potential in the absence of synaptic inputs. We found that bath-application of thapsigargin, a selective blocker of endoplasmic reticulum calcium-ATPase[52] greatly reduced calcium transients of M neurons (Figure S6H). Moreover, in current-clamp recordings, plateau potentials were completely abolished by thapsigargin (Figures 6F and 6G) and knockdown of IP_3

receptors decreased the amplitude, duration and frequency of plateau potentials (Figures 6C and 6G). These results indicate that generation of plateau potentials relies on calcium release from internal stores (Figure 6H). On the other hand, termination was suggested to be regulated by binding of internally released calcium ions to calcium- and/or voltage-dependent potassium channels, since plateau potentials were also eliminated by a potassium channel blocker tetraethylammonium (TEA; Figures 6F–6H).

In sum, these results collectively suggest that M neurons periodically produce plateau potentials via release of calcium from internal stores during early motor development.

Intrinsic activities in M neurons are required for the induction of rudimentary muscle contractions and proper motor development

We next asked whether spontaneous activities generated by M neurons induce muscular contraction and thus activate proprioceptors. We analyzed the local contractions occurring prior to the appearance of patterned motor activities (16.5 to 17.5 h AEL) as these events can contribute to activating the proprioceptive system and thus the early development of motor circuits (Figure 7A). The number of muscular contractions was greatly reduced when plateau potentials were suppressed in M neurons by knockdown of IP_3 receptors (Figure S7F, top), suggesting that M neurons induce muscle contractions.

These contractions, however, likely include those that are not driven by neurons: as noted above, part of muscular contractions occurring at this embryonic stage are generated autonomously by muscles[3]. To isolate these muscle-autonomous events, we measured the number of muscular contractions that remained in *GluRIIC* mutants.

We subtracted this number from the total number of contractions seen in control and IP_3R-knockdown embryos (Figure S7F, bottom) to estimate the extent of neurally-driven contractions, and found that it was substantially smaller in IP_3R-knockdown embryos as compared to control (Figure 7B).

Since we knocked down IP_3 receptors in both M and A27h neurons, the observed defects in muscle contractions might have resulted from decreased excitability in A27h premotor interneurons. We therefore examined their physiological properties and found that they were not affected by knockdown of IP_3 receptors (Figures S7G and S7H). We also used optogenetics with the M-specific *M-split-Gal4* to study if activation of M neurons alone is sufficient to induce muscle contractions. Light application significantly increased the frequency of muscular contractions in the embryos expressing Chrimson in M neurons (Figure 7C). These results strongly suggest that plateau potentials in M neurons serve as a major source for local muscle contractions during early motor development. Importantly, loss of these spontaneous activities in both A27h and M neurons (*R36G02* > $ip3R^{RNAi}$) or in M neurons alone (*M-split* > $ip3R^{RNAi}$) also compromised motor development: peristaltic locomotion of IP_3R-knockdown larvae was significantly slower than that in the control (Figure 7D).

A critical period for the requirement of M/A27h neural activities in motor development

Finally, we asked when M/A27h neural activities are required in the development of motor circuits. For this, we performed temporal knockdown of ShakB or IP_3 receptors by using the temperature-sensitive Gal80 repressor[53]. We found that knockdown of either gene only during late embryonic development (16-20 h AEL, when M/A27h spontaneous activities were observed) compromised larval locomotion (Figure 7E,

Pattern 1). By contrast, no such effect was seen when the knockdown was conducted outside this time window (Figure 7E, Pattern 2). These results suggest that spontaneous activity or electrical transmission in the M/A27h circuit is no longer required once the CPGs are established and thus reveal a critical period. We also asked if excessive activities in the circuit perturb motor development. Previous work in *Drosophila* embryos reported that neuronal hyperexcitability during a critical period (17-19 h AEL), which matches the timing of emergence of patterned CPG activities observed in this study (Figure 7A), causes persistent seizure-like behavior[54]. We examined if similarly manipulating excitability of the M/A27h circuit around this time window alters motor development. We employed optogenetics to periodically activate the circuit in two different patterns and found that the stride duration was prolonged in each case (Figure 7F). Thus, both inhibition and hyperexcitation of the M/A27h circuit during the critical period perturb CPG development.

Taken together, our results show that the intrinsically active M/A27h circuit self-organizes via proprioceptive experience and controls motor development (Figure 7G).

DISCUSSION

Regulation of CPG development by proprioceptive feedback

It is well established that proprioceptive feedback modulates the function of CPGs in mature motor circuits[19,20]. For instance in mice, genetic attenuation of proprioceptive feedback disrupts interjoint and flexor-extensor coordination during walking[55,56]. In *Drosophila* larvae, acute inhibition of proprioceptors greatly reduces the speed of peristaltic crawling[31,32]. Proprioceptive feedback is also known to regulate the development of synaptic connections in the somatosensory system[23,57] and premotor circuits[58]. However, the role of proprioceptive sensory feedback in sculpting locomotor

circuits has remained unclear. Previous studies in *Drosophila* indirectly studied the development of locomotory network by observing muscular movements in mutant embryos that partially lack sensory inputs, and showed that they are required for generating normal patterns of locomotion[32,59]. Here, we directly recorded CPG activities in mutants in which function or activation of all larval proprioceptors are compromised[31,32,36–38], and demonstrated for the first time that proprioceptive experience is essential for the functional maturation of locomotor CPGs (Figure 1).

Electrical synapse as a target of proprioceptive feedback

We identified modulation of electrical synapses in the M/A27h circuit as a mechanism by which proprioceptive feedback regulates CPG development. The formation of transient electrically coupled networks is a common feature of developing nervous systems[46]. Particularly in the motor system, electrically driven synchronized activities among a small group of neurons are observed prior to the formation of chemically-driven larger circuits coordinating body movements in many species including leech, fish, frogs and mice[10–15]. In zebrafish, such early activities in electrically coupled circuits have been implicated in the assembly of motor circuits for swimming[7–9,14]. However, whether and how the development of electrically coupled circuits is regulated by proprioceptive experience has been unknown. Here we show that proprioception regulates the formation of electrical coupling among the M/A27h circuit (Figure 4), which in turn is essential for the development of CPGs for larval crawling (Figure 3). Disrupting electrical coupling just in the two pairs of neurons out of several hundred in each neuromere had deteriorating effects on motor development, indicating central roles played by electrical communications among these neurons. Since A27h neurons are known to participate in the generation of peristalsis in the mature larva[25,27,

[28], it raises the possibility that the M/A27h electrical circuit serves as a scaffold which would later recruit larger motor ensembles[25]. These results support a model in which proprioceptive feedback regulates the formation of CPG circuits by strengthening electrical coupling among the core pioneer circuit mediating synchronized activities, which is required for the subsequent development of chemically-driven CPG circuits. Consistent with this view, we also observed decreased EPSPs in *nompC* mutants or when gap junctions were knocked-down in the M/A27h circuit (Figure 5). The molecular mechanism of how proprioceptive feedback regulates the formation of gap junctions remains to be determined. It could be mediated at the level of transcriptional/translational[60] or via activity-dependent modification of existing gap junction proteins[46,61–64].

Experience-dependent motor development by feedback regulation of spontaneously active neural circuits

Premature movements are observed in both vertebrates and invertebrates, suggesting the possibility that they serve conserved roles in the development of motor circuits. However, their mechanistic origin and actual roles in motor development have been hard to uncover in complex nervous systems[17,65,66]. We identified pacemaker-like activities in M neurons as a source of spontaneous activities in the nascent motor circuits in *Drosophila* (Figure 6). We also showed that M neurons' pacemaking activity is required for inducing muscular contractions and the proper development of peristaltic locomotion of the larvae (Figures 7B–7D). These results support a model of self-organized motor development via proprioceptive feedback (Figure 7G). The plateau potential in M neurons was driven by calcium release from the internal stores triggered by IP_3 signaling. Similar IP_3-mediated mechanisms have also been

implicated in the generation of spontaneous activities in the early postnatal neocortex[43,67]. How IP_3 signaling is elicited in M neurons in the absence of synaptic inputs remains to be investigated. The signaling may be triggered by intrinsic activities of the upstream G protein-coupled receptors[68], amplified through a positive feedback loop[69], and stabilized to be rhythmic because of the bell-shaped dependence of IP_3 signaling on intracellular calcium concentration[70]. Because IP_3 can diffuse to other neurons through gap junctions, synchronized activities in the M/A27h circuits may be mediated by diffusion of biochemical rather than electrical signaling via gap junctions, as has been proposed in the neocortex[43,67].

Synchronized spontaneous activities are widely seen in developing nervous systems[71]. In the sensory system, spontaneous activities and sensory experience are known to fine-tune the initially coarse sensory maps that are genetically-wired[72–74]. For instance, in the visual system, both spontaneous activities in retinal ganglion cells (so-called retinal waves) and visual inputs are required for the refinement of retinotopic and eye-specific maps in the brain[75–78]. Similarly, in the somatosensory cortex, spontaneous activities are observed prior to the onset of peripheral afferents. These activities are derived from a specific region (thalamic nuclei) and spatially propagate to neighboring regions via gap junctions[79]. Recent progress has uncovered that either disruption of spontaneous activities or sensory deprivation impairs the later development of the somatosensory system[72,79,80]. These studies together suggest that the general process of circuit maturation is remarkably similar across various brain regions. Similarly, we show here that both spontaneous activities and proprioceptive afferents are necessary for the proper development of the motor system in *Drosophila*. However, unlike in the sensory system where environmental stimuli drive afferent inputs independently of spontaneous activities, proprioceptive afferent inputs are

internally produced by the spontaneous motor activities. We propose that a pioneer CPG circuit in *Drosophila* embryos use sensory 'echoes' of their own intrinsic outputs to assemble a functional locomotor network (Figure 7G). During this process, M and A27h neurons may function as intersegmental scaffolds that recruit and bridge other local neurons for them to act in concert. The long duration of M neuron's plateau potential and slow propagation of IP_3 signaling along the neuromeres allow ample time for the cohort of local neurons and afferent inputs to be coactive so that their connections can be strengthened, for instance, by a Hebbian mechanism. In zebrafish, intersegmental neurons generating plateau potentials[48] have been implicated in intersegmental integration of activities in nascent motor circuits[8]. It will be interesting to examine if there exists a conserved learning rule that optimizes the functional wiring for locomotor circuitry.

ACKNOWLEDGMENTS

We would like to thank Hiroshi Kohsaka for technical advice and providing the fly stocks; Yuh Nung Jan, Aaron DiAntonio and Bloomington Drosophila Stock Center for providing fly stocks; Matthias Landgraf, and members of Kazama laboratory for their comments on the manuscript; members of Nose and Kazama laboratories for their support and cooperation throughout the study. This work was supported by KAKENHI Grant-in-Aid 19H04742, 18H05113, 17H05554 to A.N., 21H04789, 18H02532 to H.K., 19J21596 (JSPS Fellows) to X.Z., and a grant from RIKEN to H.K.

AUTHOR CONTRIBUTIONS

X.Z., H.K. and A.N. designed the project and wrote the paper. X.Z. performed the experiments and analyzed the data. Y.K. helped with the behavioral experiments, immunohistochemistry, and data analysis. T.K. and K.I. provided advice and technical expertise on pan-neuronal calcium imaging experiments and electrophysiological experiments respectively. J.J. and S.R.P. generated the M-split-Gal4 transgenic fly line. H.K. and A.N. supervised the project.

DECLARATION OF INTERESTS

The authors declare no competing interests.

SUPPLEMENTAL INFORMATION

Supplemental information can be found online at https://doi.org/10.1016/j.cub.2021.10.005.

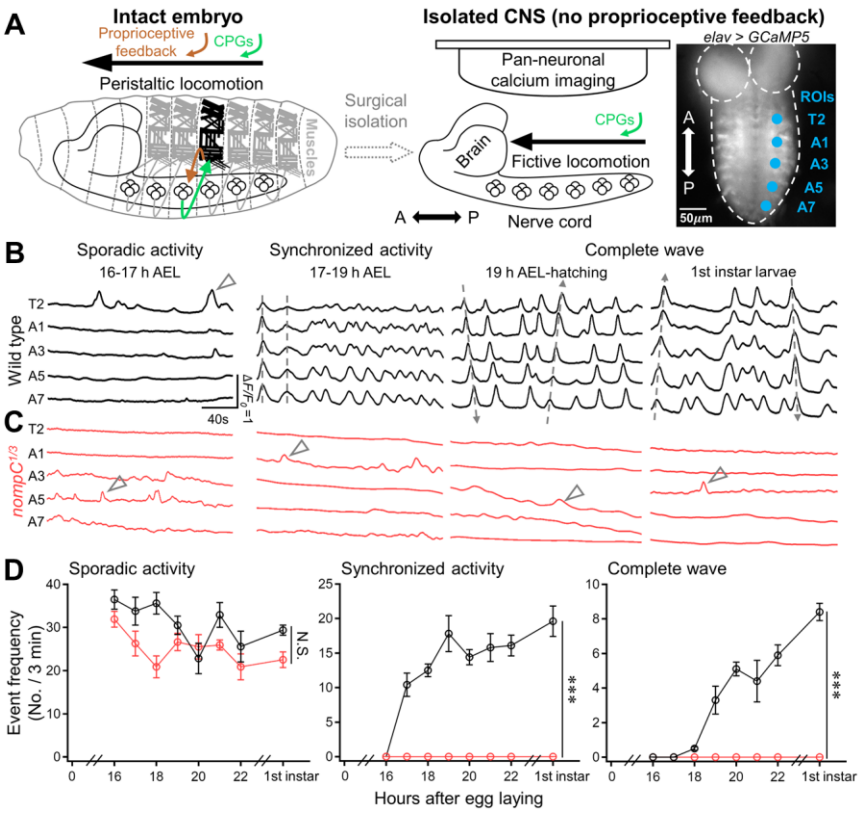

Figure 1. Proprioceptive experience is required for the functional development of locomotor CPGs

(A) A diagram showing experimental procedures for pan-neuronal calcium imaging of the isolated embryonic CNS. The right-most panel shows an actual image and regions of interest (ROIs). Dashed lines delineate the boundary of the brain and nerve cord. A, anterior; P, posterior. Note that in the intact embryo, peristaltic locomotion is regulated by the CPGs and proprioceptive feedback from muscles, whereas fictive locomotion in the isolated CNS is solely driven by the CPGs.

(B and C) Representative examples of pan-neuronal imaging in wild type (*elav-Gal4* > *UAS-GCaMP5*, B) and *nompC*$^{1/3}$ embryos (*nompC*$^{1/3}$; *elav-Gal4* > *UAS-GCaMP5*, C) at different stages. Grey arrowheads, dashed lines and arrows denote examples of sporadic, synchronized activities and complete waves, respectively. h AEL, hours after egg laying.

(D) Quantifications of the three types of activities during development. n = 6, 4, 4, 8, 5, 4, 4, 18 and 5, 3, 3, 6, 4, 5, 5, 34 for wild type and *nompC*$^{1/3}$ embryos at each stage. Note that only

sporadic activities were seen in *nompC*$^{1/3}$ mutants. Two-way ANOVA. ***$P < 0.001$, **$P < 0.01$, *$P < 0.05$, N.S., not significant and error bars indicate s.e.m. in this and the following figures. See also Figure S1.

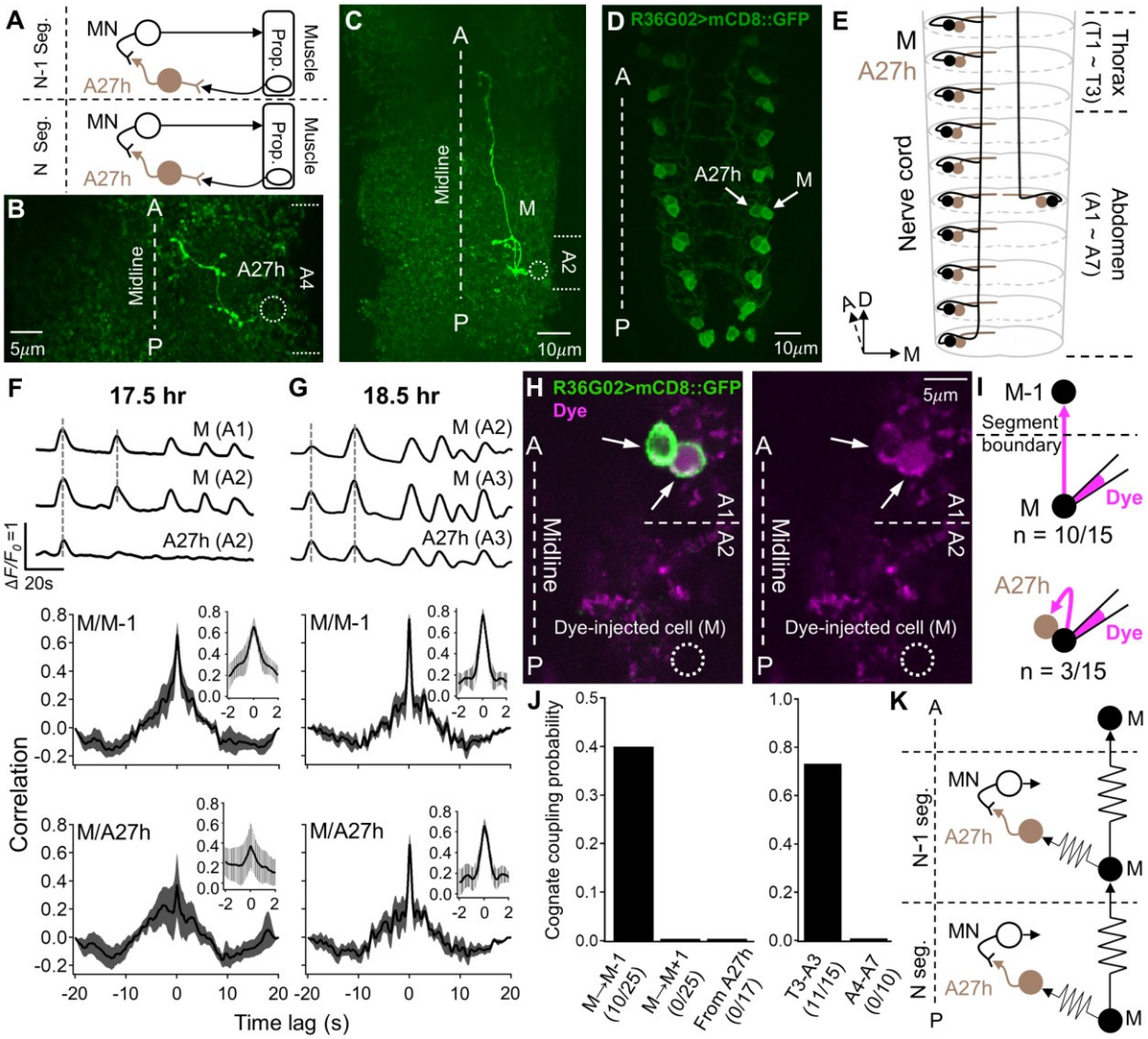

Figure 2. M and A27h neurons form gap-junctionally coupled circuits generating synchronized activities during early motor development

(A) A wiring diagram showing that A27h neurons receive direct input from proprioceptor (prop.) and activate motor neuron (MN)[25]. Seg., segment.

(B–E) Morphology of M and A27h neurons. (B and C) Morphology of single A27h (B) and M neurons (C) revealed by biocytin injection. Dashed circles indicate the positions of the somata that were detached after the dye injection. (D) Expression pattern of *R36G02-Gal4*. M and A27h neurons in the same hemineuromere are always closely apposed with their initial axon segments fasciculated, suggesting that they are sibling neurons. (E) A digram showing the morphology of M and A27h neurons in the nerve cord. A, anterior; D, dorsal; M, medial. Only

one each of M and A27h neurons are shown on the right side of the diagram, to reveal their neurite extension pattern.

(F and G) Examples of calcium imaging (top) and average cross-correlation functions of synchronized activities (bottom) in neighboring M neurons (M/M-1) and M and A27h neurons (M/A27h) at 17.5 hours (F, n = 5) and 18.5 hours (G, n = 8). The grey bands represent ± s.e.m. across embryos. Insets, expanded view.

(H) An example of cognate coupling.

(I) Schematic summary of cognate couplings from M to one anterior M neuron and A27h neuron. Counted from T3-A3 neuromeres since cognate coupling was never seen when dye was injected into M neurons in A4-A7 neuromeres (J, right).

(J) Left: cognate coupling probabilities from M to the next anterior M (M-1), M to the next posterior M (M+1) and from A27h to cognate neurons. Right: probabilities of coupled cognate cells seen in anterior (T3-A3) and posterior (A4-A7) neuromeres.

(K) Schematic wiring diagram of electrically coupled M/A27h circuits. Unidirectional resistors indicate rectifying electrical connections.

See also Figures S2 and S3.

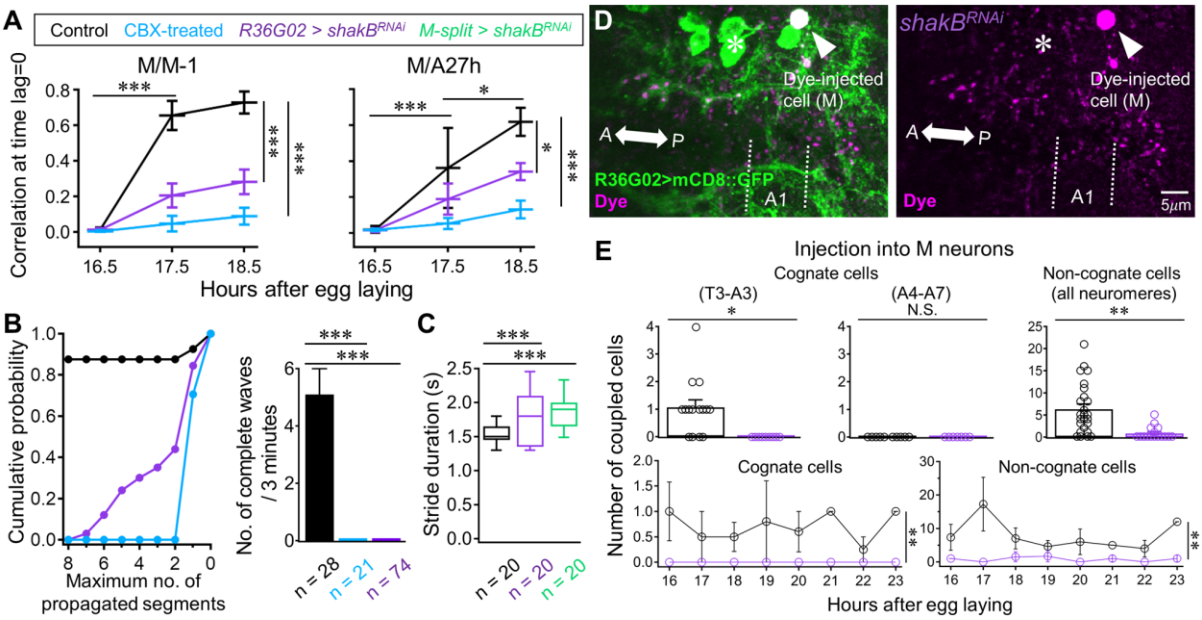

Figure 3. Gap-junctional transmission mediated by ShakB in the M/A27h circuit is required for motor development

(A) Quantification of correlation coefficient at time lag = 0 (as it reflects the strength of sychronized activities) in wild type (n = 5, 5, 8 for embryos at 16.5, 17.5 and 18.5 h AEL), CBX-treated (n = 3, 4, 8) and *shakB*^{RNAi} (n = 4, 6, 5) embryos. *R36G02-Gal4* > *UAS-GCaMP6m* embryos in saline were used as a control. Two-way ANOVA followed by Tukey's *post hoc* analysis.

(B) Cumulative plot of maximum number of segments through which fictive wave-like activities propagated (left) and quantification of the number of complete waves (right). Only partial waves occurred in *shakeB*^{RNAi} individuals and no wave at all in the presence of CBX. 19-30 h AEL embryos/larvae were used. Mann–Whitney *U*-test followed by Holm–Bonferroni correction.

(C) Quantification of stride duration of newly hatched larvae. *UAS-shakB*^{RNAi}/+ larvae were used as a control. Two-tailed Student's t-test followed by Holm–Bonferroni correction. Boxplots indicate the median, 25th, 75th percentiles and whiskers above and below the box indicate the 90th and 10th percentiles respectively, in this and the following figures.

(D) An example of dye-coupling following injection into an M neurons in the ShakB-knockdown embryo *(R36G02-Gal4 > UAS-shakB^{RNAi}*). Note that dye did not diffuse to any other cell bodies. (E) Top: quantifications of cognate coupling in T3-A3 neuromeres (left, n = 15, 9 embryos/larvae for wild type and *shakB^{RNAi}* respectively) or in A4-A7 neuromeres (middle, N = 10, 7) and that of non-cognate coupling in all neuromeres (right, N = 25, 16), following dye injection into M neurons in wild type and *shakB^{RNAi}* embryos. Mann–Whitney *U*-test. Bottom: quantifications of cognate coupling (left) and non-cognate coupling (right) against developmental stages. n = 3, 2, 4, 5, 5, 1, 4, 1 and 1, 2, 2, 3, 2, 2, 2,2 for wild type and *shakB^{RNAi}* embryos at each stage. Two-way ANOVA.

See also Figure S4.

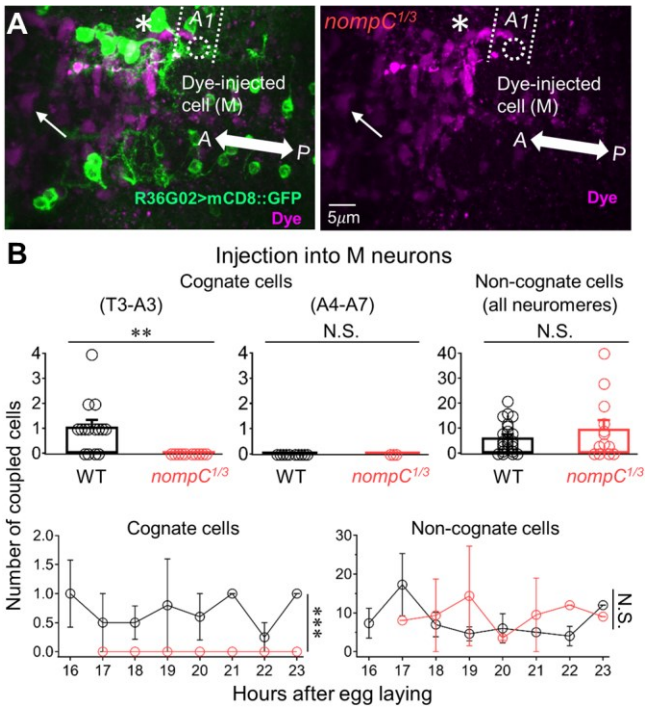

Figure 4. Cognate coupling in the M/A27h circuit is abolished in *nompC* mutants

(A) An example of dye coupling following injection into an M neuron in *nompC*$^{1/3}$ embryo. Dashed circles indicate the position of the soma that was detached after the dye injection. Note that dye diffused to non-cognate (arrow) but not cognate cells in the next anterior segment (asterisks).

(B) Top: quantifications of cognate coupling in T3-A3 neuromeres (left, n = 15, 10 embryos/larvae for wild type and *nompC*$^{1/3}$ respectively) and in A4-A7 neuromeres (middle, n = 10, 3) and those of non-cognate coupling in all neuromeres (right, n = 25, 13), following dye injection into M neurons in wild type (black) and *nompC*$^{1/3}$ mutants (red). Mann–Whitney *U*-test. Bottom: quantifications of cognate coupling (left) and non-cognate coupling (right) against developmental stages. n = 3, 2, 4, 5, 5, 1, 4, 1 and 1, 3, 3, 2, 2, 1, 1 for wild type and *nompC*$^{1/3}$ embryos at each stage. Two-way ANOVA (17-23 h AEL).

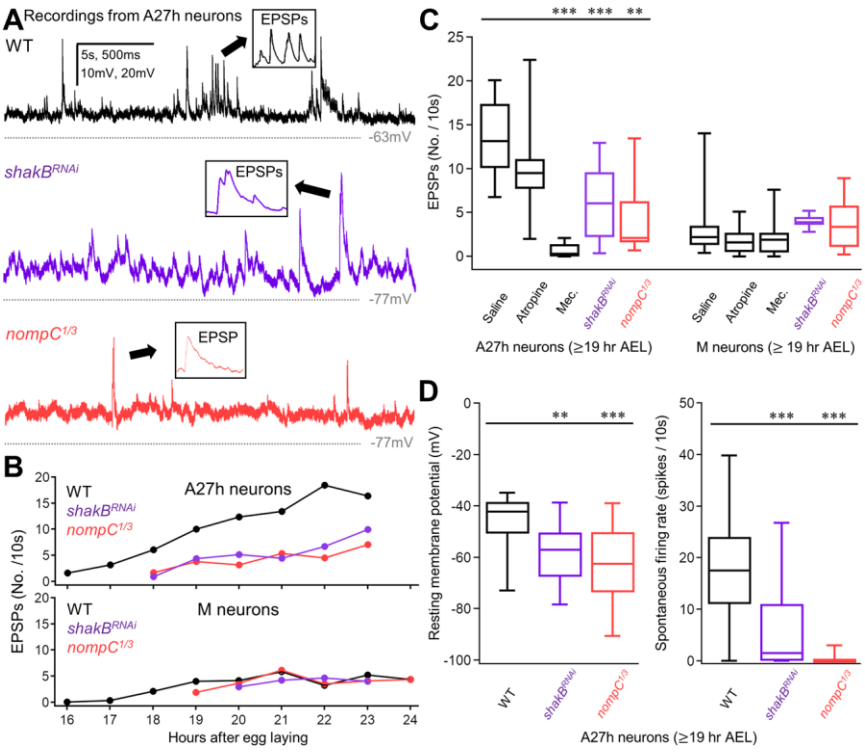

Figure 5. Chemical synaptic input to and spiking output from A27h neurons are impaired in the absence of electrical coupling or proprioception

(A) Representative traces of current-clamp recordings from A27h neurons in each genotype.

(B) Plots of mean frequencies of EPSPs against developmental stages in A27h (top, n ≥ 5, 4, 3 for wild type, *shakB*^{RNAi}, *nompC*$^{1/3}$ at each stage) and M neurons (bottom, n ≥ 6, 4, 2).

(C) Quantification of EPSP frequency. Atropine and mecamylamine (Mec.) were used to block muscarinic and nicotinic acetylcholine receptors, respectively. n = 34, 5, 6, 18, 24, 53, 5, 7, 9, 32 cells from left to right (19-24 h AEL embryos/larvae). Mann–Whitney *U*-test followed by Holm–Bonferroni correction.

(D) Quantifications of the resting membrane potential (left) and spontaneous firing rate (right) of A27h neurons in each genotype. n = 34, 18, 24 cells for wild type, *shakB*^{RNAi}, *nompC*$^{1/3}$ (19-24 h AEL embryos/larvae). Mann–Whitney *U*-test followed by Holm–Bonferroni correction.

See also Figure S5.

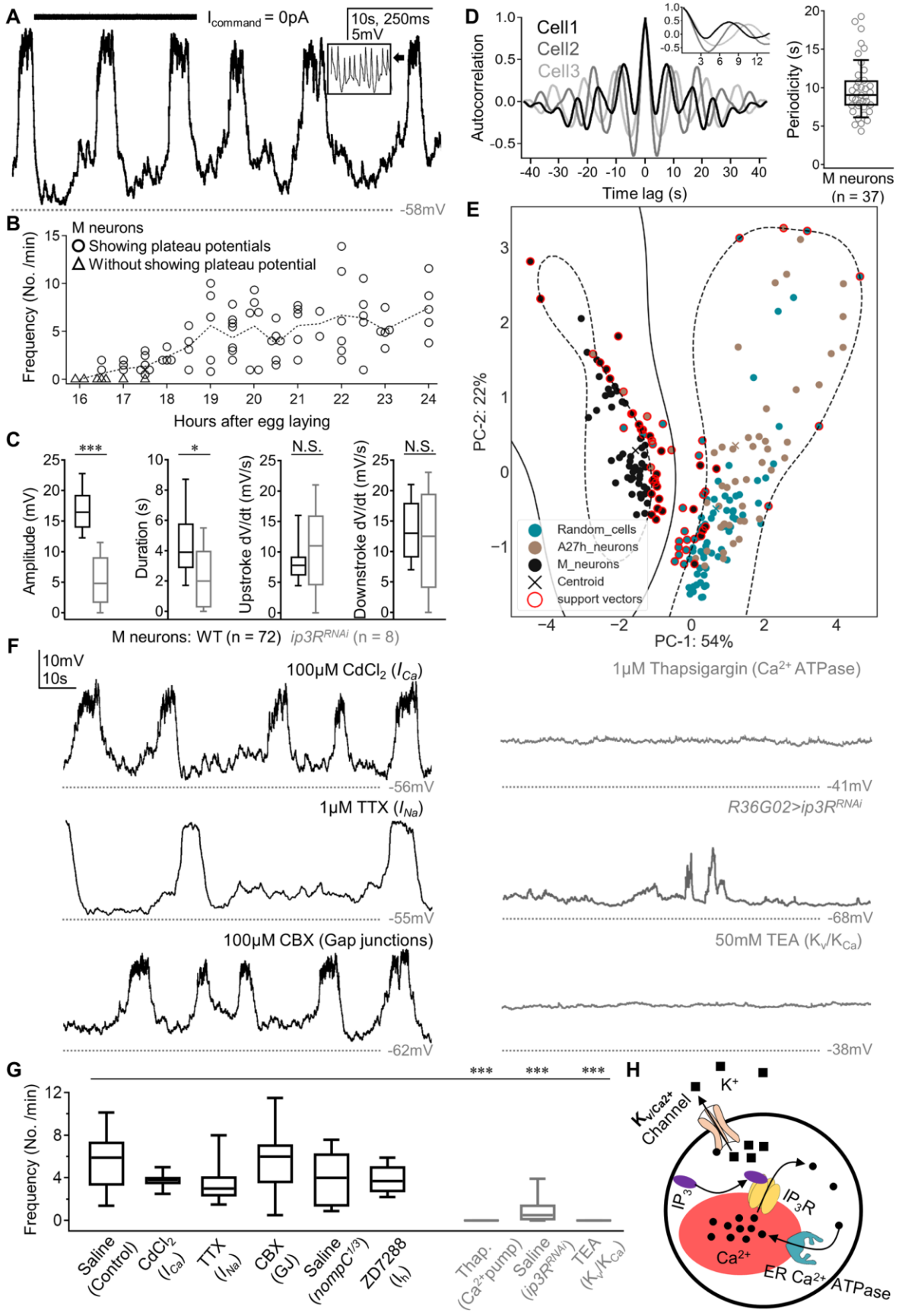

Figure 6. M neurons are capable of generating plateau potentials via internal calcium

release

(A) A typical trace of current-clamp recording from an M neuron (20.5 h AEL) generating rhythmic plateau potentials. Inset shows the action potentials during burst firing.

(B) Plot of frequency of plateau potentials against developmental stages. Dashed line indicates the mean.

(C) Activity characteristics of plateau potentials in wild type and IP_3R-knockdown (*R36G02-Gal4 > UAS-ip3R*^{RNAi}) M neurons. Mann–Whitney *U*-test.

(D) Examples of autocorrelation functions in three individual M neurons (left) and plot of periodicities of plateau potentials observed in 37 individual M neurons from 19 to 24 h AEL (right).

(E) PCA of activity characteristics of each cell type (Figure S6D). Curve and dashed curves indicate, hyperplane for a SVM classifier that separates activities of M from those of A27h or random cells, and boundaries of margins, respectively.

(F and G) Examples (H) and quantification (I) of the effect of inhibiting voltage-dependent calcium channels (I_{Ca}) ($CdCl_2$), voltage-dependent sodium channels (I_{Na}) (TTX), gap junctions (CBX), endoplasmic reticulum calcium-ATPase (Thapsigargin), IP_3 receptors (*ip3R*^{RNAi}), voltage- and calcium-dependent potassium channels (K_v/K_{Ca}) (TEA), proprioception (*nompC*$^{1/3}$) and hyperpolarization-activated inward currents (I_h) (ZD7288). Manipulations that significantly affected the frequency of plateau potentials are marked in grey. n = 52, 5, 7, 7, 23, 4, 7, 8, and 5 from left to right (19-24 h AEL embryos/larvae). Mann–Whitney *U*-test followed by Holm-Bonferroni correction.

(H) Model of how M neurons generate plateau potentials via releasing internal calcium stores. Solid black circles and squares indicate calcium and potassium ions respectively.

See also Figures S6 and S7.

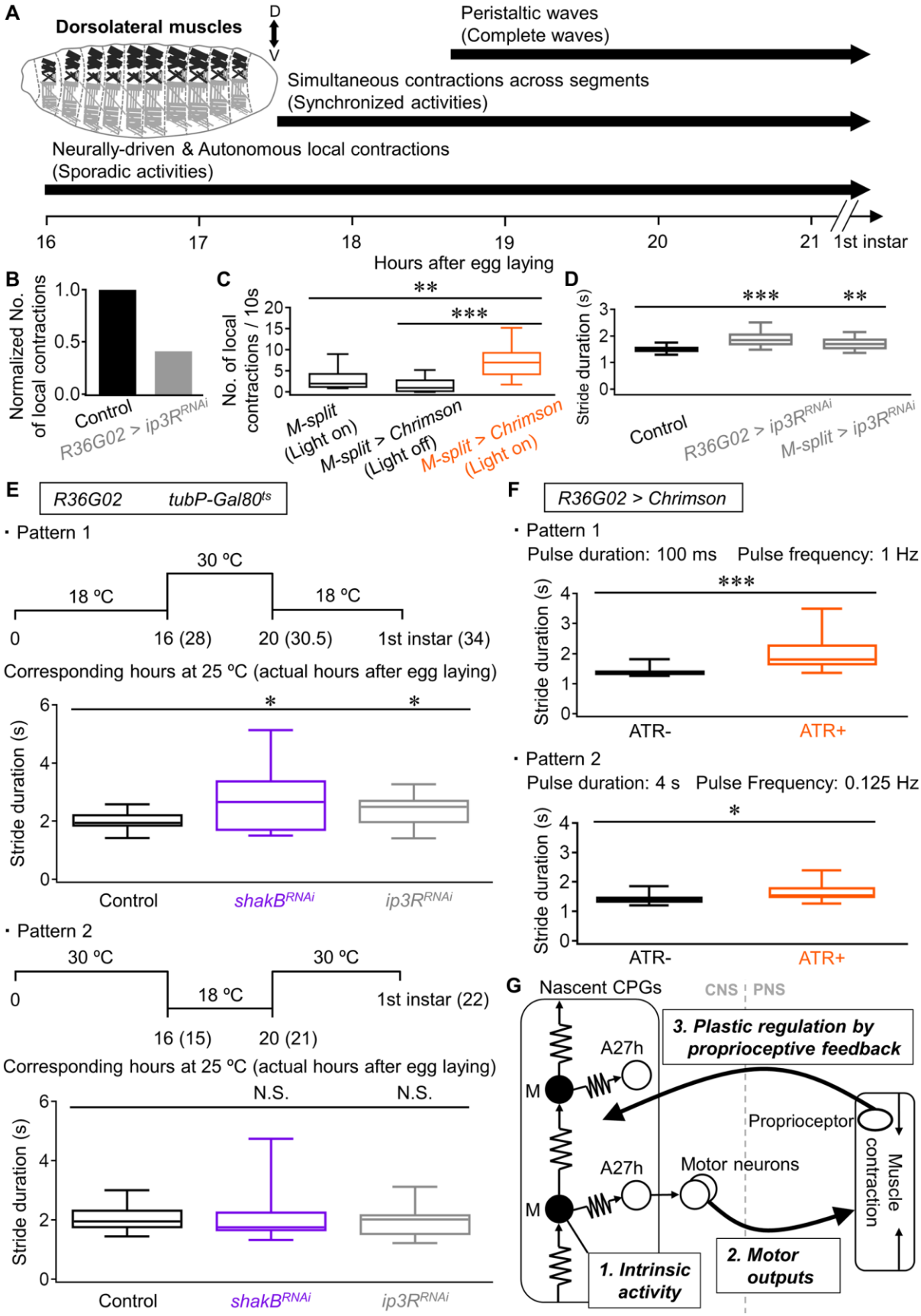

Figure 7. Activities of M neurons during a critical period are required for generating

rudimentary muscle contractions essential for motor development

(A) Timeline summary showing the emergence of each motor behavior (corresponding CPG patterns are indicated in parentheses) during late embryogenesis. To quantify rudimentary movements, local contractions (including neurally-driven and muscle autonomously generated) of the dorsolateral muscles (highlighted in black) from 16.5 to 17.5 h were recorded (B and C).

(B) Level of neurally-driven local muscle contractions observed during 16.5-17.5 h AEL in IP_3R-knockdown embryos normalized to that in the control (for details, see Figure S7F).

(C) Quantification of the number of local contractions in controls (*M-split*, light on; *M-split* > *Chrimson*, light off) and *M-split* > *Chrimson* embryos. For light-on groups, a 10-second light stimulation was delivered twice at an interval of 30 seconds. For light-off group, muscle contractions occurring 10 seconds prior to the stimulation were counted. n = 10 embryos (20 trials) for each group (16.5-17.5 h AEL embryos). Mann–Whitney *U*-test followed by Holm–Bonferroni correction.

(D) Quantification of stride duration in control (*UAS-ip3R*^{RNAi}/+) and IP_3R-knockdown newly hatched larvae. n = 20 larvae for each group. Two-tailed Student's t-test followed by Holm–Bonferroni correction.

(E) Experimental procedures of temporal knockdown and quantifications of stride duration of newly hatched larvae after temporal knock-down of ShakB and IP_3R. TubP-Gal80^{ts} suppresses the transcriptional activation by Gal4 at 18 °C but relieves the suppression at 30 °C. n = 20 larvae for each group. Two-tailed Student's t-test followed by Holm–Bonferroni correction.

(F) Quantifications of stride duration of newly hatched larvae following chronic optogenetic stimulations from 17 to 19 h AEL. Pulse duration and frequency of Pattern 1 and 2 were based on the protocol reported previously[54] and the characteristics of M neurons' plateau potentials (Figures 6C and 6D), respectively. Embryos whose parental flies were not fed with all-trans

retinal (ATR) but received the same light stimulation were used as control (ATR-). n = 20 larvae for each group. Two-tailed Student's t-test.

(G) A model of motor development through an interplay between spontaneous motor activity and proprioceptive feedback. During an early phase of motor development, pacemaker M neurons generate intrinsic activities via IP_3-mediated Ca^{2+} release from internal stores and activate premotor A27h neurons via gap junctions (1), which then activate motor neurons inducing muscular contraction (2). Proprioceptors are activated by muscle contraction and provide proprioceptive feedback essential for maturation of the M/A27h circuit (3) and eventually for generating coordinated movements.

See also Figure S7.

STAR★METHODS

RESOURCE AVAILABILITY

Lead Contact

Further information and requests for resources and reagents should be directed to and will be fulfilled by the Lead Contact, Akinao Nose (nose@k.u-tokyo.ac.jp).

Materials Availability

Data and materials that support the findings of this study are available from the Lead Contact upon request.

Data and Code Availability

Data reported in this paper have been deposited in https://doi.org/10.17632/mh3nzy64nc.1. This study did not generate any unique code.

EXPERIMENTAL MODEL AND SUBJECT DETAILS

Fly Stocks

The following fly strains were used in this study: *yw* (Bloomington stock no. 6598), *nompC*^{1} and *nompC*^{3} [37], *Mhc*^{1} [40], *GluRIIC*[41], *2-21-GAL4*[31], *elav-GAL4*[81], *nSyb-GAL4* (Bloomington stock center no. 58763), *R36G02-GAL4* (Bloomington stock no. 49939)[25], *M-split-GAL4 (tsh−p65ADZp; VT002081-ZpGdbd), UAS-mCD8::GFP* (Bloomington stock center no. 32186), *UAS-GCaMP5* (Bloomington stock center no. 42038), *UAS-GCaMP6m* (Bloomington stock center no. 42750), *UAS-CD4::GCaMP6f*[26], *UAS-CsChrimson::mVenus* (Bloomington Stock Center no. 55136), *tubP-GAL80*^{ts} (Bloomington Stock Center no. 7019), *UAS-shakB*^{RNAi}

(Bloomington stock center no. 57706), *UAS-ogre*^{RNAi} (Bloomington stock center no. 44048), *UAS-innexin2*^{RNAi} (Bloomington stock center no. 42645), *UAS-innexin3*^{RNAi} (Bloomington stock center no. 30501), *UAS-innexin4* (zpg)^{RNAi} (Bloomington stock center no. 35607), *UAS-innexin5*^{RNAi} (Bloomington stock center no. 30501), *UAS-innexin6*^{RNAi} (Bloomington stock center no. 44663), *UAS-innexin7*^{RNAi} (Bloomington stock center no. 26297), *UAS-TeTxLC* (Bloomington stock center no. 28838), *UAS-ip3R (Itpr)*^{RNAi} (Bloomington stock center no. 51686). *UAS-Dicer2* (Bloomington stock center no. 24650) was co-expressed with the RNAi constructs for efficient knockdown of innexins.

All experiments in this study were conducted with embryos and newly hatched larvae (ages ≤ 30 h AEL except for those shown in Figure 7E) at room temperature (25°C) unless otherwise noted. For accurate staging, eggs were collected for 20 minutes from parental flies raised in a cup at 25˚C covered with an yeast-pasted agar plate.

METHOD DETAILS

Behavioral Assay of Embryos and Newly Hatched Larvae

Embryos were dechorionated and placed in halocarbon oil (H8898, Sigma) to prevent dehydration during long-term recordings. Videos were recorded by a stereomicroscope (SZX16, Olympus, Japan) equipped with an XCD-V60 CCD camera (15 frames/second). Movies were downloaded into VFS-42 (Vision Freezer, Chori imaging) for statistical analyses. To quantify local contractions in 16.5-17.5 h AEL embryos (Figures 7B, 7C, and S7F), the entire length of an embryo was divided into ten partitions with equal length mannually. Contractions of dorsolateral muscles within two partitions are regarded as local movements.

Newly hatched larvae were gently washed in distilled water and then placed on an apple-juice agar plate. After a 3-minute acclimation, the crawling movements were recorded for 1 minute by a stereomicroscope (SZX16, Olympus, Japan) equipped with an XCD-V60 CCD camera (30 frames/sec). The number of larval peristalses (sequential muscular contractions across all segments) was manually counted by using ImageJ software (National Institute of Health). Stride duration was calculated as the average time needed for accomplishing a single forward peristalsis.

Calcium Imaging of the Isolated CNSs

Dissection was carried out in the following steps: 1. embryos were devitellinized on a double-sided tape (NW-K15, Nichiban) by using a glass capillary (Calibrated Micropipettes 10 or 20 μL, Drummond, U.S.A., for newly hatched larvae, this step was skipped); 2. embryos or larvae were placed dorsal-side-up and fixed on the surface of the double-sided tape with glue (3M Vetbond) at head and tail ends; 3. an incision along the dorsal cuticle was made using the glass capillary; 4. internal organs were removed to expose the CNS; 5. all peripheral nerves were cut off and the CNS was isolated from the body wall (for experiments in Figures S1A–S1D, this step was skipped). Dissections and experiments were carried out in physiological saline containing 135 mM NaCl, 5 mM KCl, 2 mM $CaCl_2$, 4 mM $MgCl_2$, 5 mM TES, and 36 mM sucrose (pH = 7.2)[82]. The dissection procedure generally took ~3 minutes.

Immediately after dissection, uniform blue light from the Xe lamp (X-Cite, Excelitas Technologies) was applied onto the preparation and GCaMP signals were detected by an EMCCD camera (iXon3, ANDOR Technology) through a standard GFP filter unit. Neural activities in the entire nerve cord were imaged with a water-immersion objective

lens (40X or 60X, Zeiss Achroplan) at a rate of 20 frames/second for 3 minutes (3600 frames).

Calcium imaging data were analyzed by using ImageJ software. The change in signals were normalized with baseline fluorescent intensity ($\Delta F/F_0$) and only signals higher than one standard deviation of the baseline fluctuation were regarded as calcium events. *elav-Gal4* and *nSyb-GAL4* were used for pan-neuronal calcium imaging (Figures 1, S1E, and S1F), ROIs were set on the neurites of five spatially segregated neuromeres (T2, A1, A3, A5 and A7, neuromere arrangement identified by the characteristic positions of five motor neurons on the dorsal side[83]). For detecting calcium activities of M and A27h neurons (Figures 2F, 2G, S2B and S2C), embryos or larvae carrying *R36G02-Gal4* > *UAS-GCaMP6m* were used. ROIs are indicated in each figure panel except for the data in Figure 3B and Figure S4E, where 8 ROIs were set on either somata or neurites of M and A27h neurons from T3 to A7 neuromeres. When ROIs were set on somata, the correspondence between axonal and somatic activity was used to determine the identity of somata, since axons of M and A27h neurons are morphologically distinguishable. Synchronized activity was defined as simultaneous increases of mean fluorescent intensities in ≥ 2 neighboring ROIs (delay of peak fluorescent intensities < 0.1 second); complete wave was defined as sequential increases of mean fluorescent intensities throughout the entire five ROIs in pan-neuronal imaging or eight ROIs in calcium imaging of M and A27h neurons (delay of neighboring ROIs > 0.5 but < 5 seconds); sporadic activity is defined as an episodic event that either occurred in a single ROI or in multiple non-contiguous ROIs. The cross-correlation function described in Figures 2F, 2G, 3A and S4D was defined as

$$CCF_{xy}(\tau) = \frac{\sum_{t=0}^{T}(x(t) - \bar{x})(y(t-\tau) - \bar{y})}{\sqrt{\sum_{t=0}^{T}(x(t) - \bar{x})^2 \sum_{t=0}^{T}(y(t-\tau) - \bar{y})^2}}$$

where $x(t)$ and $y(t)$ represent calcium activities (changes of fluorescent intensities over time) of cell A and B respectively, $\bar{x}$ and $\bar{y}$ the means of corresponding series, τ the time lag of $y(t)$ relative to $x(t)$ and T the time duration of each trial.

Immunohistochemistry

The following primary antibodies were used: rabbit anti-GFP (Af2020, Frontier Institure; 1:1000; RRID: AB 10615238), mouse anti-ChAT (4B1, Hybridoma Bank; 1:50; RRID: AB 528122), Cy5-conjugated goat anti-HRP (Life Technologies; 1:300; RRID: AB 2338967). The following secondary antibodies were used: goat Alexa Fluor 488-conjugated anti-rabbit IgG (A-11034, Invitrogen Molecular Probes; 1:300; RRID: AB 2576217), goat Alexa Fluor 555-conjugated anti-mouse IgG (A-21424, Invitrogen Molecular Probes; 1:300; RRID: AB 141780).

Embryos or newly hatched larvae were dissected as described above and immunostained in the following steps: 1. the preparations were washed with phosphate buffered saline (PBS) and fixed in 4% paraformaldehyde (dissolved in PBS) for 30 minutes at room temperature; 2. they were washed with 0.2% Triton X-100 in PBS (PBT) for 30 minutes (15-minute wahsing for two times); 3. they were then incubated with 5% normal goat serum (NGS) in PBT for 30 minutes; 4. they were incubated overnight at 4°C with the primary antibodies; 5. they were washed as in step 2, then incubated overnight at 4°C with the secondary antibodies. Fluorescent images were acquired by using a confocal microscope (FV1000, Olympus) equipped with 40X, 60X and 100X water-immersion objective lens (Olympus LUMPlanFI).

Whole-cell Recording and Dye Injection

Embryos or newly hatched larvae were dissected as described above in the external saline containing 103 mM NaCl, 3 mM KCl, 5 mM *N*-Tris (hydroxymethyl) methyl-2-aminoethane-sulfonic acid (TES), 8 mM trehalose dehydrate, 10 mM glucose, 26 mM $NaHCO_3$, 1 mM NaH_2PO_4, 1.5 mM $CaCl_2$, and 4 mM $MgCl_2$ (pH = 7.2, osmolarity = 275 mOsm[84]). The preparation was continuously perfused with the external saline, bubbled with 95% O_2 and 5% CO_2 throughout the recording. For whole-cell patch-clamp recording, a patch pipette was pulled from a thin-wall glass capillary (resistance of the pipettes is 14 ($\pm$3) MΩ; 1.5mm o.d./ 1.12 mm i.d., TW150F-3, World Precision Instruments) and filled with internal solution containing 140 mM KOH, 140 mM aspartic acid, 10 mM HEPES, 1 mM EGTA, 4 mM MgATP, 0.5 mM Na_3GTP, and 1 mM KCl (pH = 7.2, osmolarity = 265 mOsm[84]). Either 0.5% biocytin hydrazide (AAT Bioquest) or 2% neurobiotin (Vector Laboratories) was included for visulazing cell morphology and testing dye coupling respectively. Recordings were made with a Multiclamp 700B amplifier (Molecular Devices) equipped with a CV-7B headstage. Signals were low-pass filtered at 2 kHz and digitized at 10 kHz. At voltage-clamp mode, the cell was clamped at -60 mV and spontaneous EPSCs were recorded (Figure S5E), then a negative square-current pulse (10 mV, 200 ms) was injected into the cell for determining input resistance (average of 10 consecutive sweeps; Figure S5A). Voltage steps of 10 mV increment were applied to the cell from -90 to 40 mV to calculate the voltage-current relationship (average of 3 consecutive sweeps at each step; Figure S5D). Current-clamp mode was used for recording spontaneous activity and assessing the firing rate (by injecting positive step currents, average of 3 consecutive sweeps; Figures S5B and S5C), the resting membrane potential (membrane potential at $I_{command}$ = 0 pA, average of 10 consecutive sweeps; Figures 5D and S5A), the spotaneous firing rate (Figure 5D), and the spiking threshold (the average membrane

potential of 3 sweeps in which single action potentials were evoked; Figures S5C, S7G, and S7H). Recordings were made from one cell per embryo or larva and cells showing no activity were not used for data analysis. Raw data were acquired and analyzed by using Igor Pro 8 (WaveMetrics) unless otherwise noted. After the recording, the whole-cell configuration was maintained for ≥ 30 minutes and a gentle positive pressure was applied to let the dye diffuse into the injected and coupled cells. After retracting the patch pipette (in most cases, the soma came off with pipettes), the sample was immunostained as described above except that streptavidin: CF555 (29038, Biotium) was used for visulazing biocytin and neurobiotin. For pharmacological experiments, one of the following chemicals was bath applied to 19-24 h AEL embryos/larvae by dissolving it in the external solution containing 100 μM $CdCl_2$ (202908, Sigma), 1 μM tetrodotoxin (1069, Tocris Bioscience), 100 μM carbenoxolone (C4790, Sigma), 30 μM ZD7288 (Z3777, Sigma), 50 μM atropine (A0132, Sigma), 50 μM mecamylamine (M9020, Sigma), 1 μM thapsigargin (T9033, Sigma), and 50 mM TEA (T2265, Sigma). Only one of the above chemicals was used for each cell (Figures 5C, 6F, 6G, S5D, and S6A). In all the whole-cell patch-clamp recording and dye injection experiments, embryos and larvae carrying *R36G02-Gal4 > UAS-mCD8::GFP* were used to identify M and A27h neurons. The following characteristics were used to distinguish the two neurons when accessing the cell: 1. *R36G02-GAL4* drives stronger expression in M than A27h neurons; 2. M neurons are positioned more laterally than A27h neurons (Figures 2B–2E). The autocorrelation function of each trial in current-clamp experiments (Figure 6D) was defined as

$$ACF_x(\tau) = \frac{\sum_{t=0}^{T}(x(t) - \bar{x})(\,x(t-\tau) - \,\bar{x})}{\sqrt{\sum_{t=0}^{T}(x(t) - \bar{x})^2 \sum_{t=0}^{T}(x(t-\tau) - \,\bar{x})^2}}$$

where $x(t)$ represents spontaneous activity (changes of membrane potential over time) of M neuron ($\bar{x}$ is the mean of series), τ is the time lag and T is the duration of

each trial. Periodicity of plateau potentials is a period from $\tau = 0$ to τ of the next peak of the autocorrelation function.

To determine the characteristics of neuronal activity of a given cell, all events within the first 120-second current-clamp recording (at $I_{command}$ = 0 pA) were extracted and the average voltage amplitude, steady-state duration, frequency, time derivative of the voltage of upstroke and downstroke were calculated (Figure S6D). These data were then normalized by

$$z_i = \frac{x_i - \bar{x}}{\sqrt{\frac{1}{N-1}\sum_{i=1}^{N}(x_i - \bar{x})^2}}$$

where x_i represents one observed value, $\bar{x}$ is the mean across cells and N is the total number of events. The normalized data were used for PCA (by using the scikit-learn library in Python 3.7, Python Software Foundation). In Figure 6E, we took the two PCs with the highest proportion of variance explained as the x and y axes and plotted each cell with a coordinate. In the two-dimensional PC space, the cluster of M neurons is segregated from that of A27h neurons and random cells. To quantify the discriminability between the clusters, we trained an SVM to classify the activity patterns of M neurons from those of other cell types (A27h and randomly selected cells). We used the soft-margin technique to enhance the robustness and the tolerance to outliers in our model. The formula for finding the optimal boundary of soft-margin is given by

$$\left[\frac{1}{n}\sum_{i=1}^{N} max(0, 1 - l_i(\vec{\omega} \cdot \vec{x_i} - b))\right] + \lambda\|\vec{\omega}\|$$

where l_i is the label that indicates whether a cell is M neuron or not, $\vec{x_i}$ is the support vectors for determining the boundary of margin, $\vec{\omega}$ is the normal vector to the hyperlane, b is the bias for training and λ is used to determine the trade-off between

maximizing the margin and to ensure that the support vectors lie on the correct side of the margin. To better classify the data, we chose a nonlinear SVM classifier by using Gaussian radial basis function (RBF) kernel trick. The RBF kernel is given by

$$K(\overrightarrow{x_i}, \overrightarrow{x_j}) = \exp\left(-\frac{\left\|\overrightarrow{x_i} - \overrightarrow{x_j}\right\|^2}{2\sigma^2}\right)$$

where $K(\overrightarrow{x_i}, \overrightarrow{x_j})$ represents a kernel function, $\overrightarrow{x_i}$ and $\overrightarrow{x_j}$ represent two different vectors in the PC space, $\left\|\overrightarrow{x_i} - \overrightarrow{x_j}\right\|$ is their Euclidean distance, and σ is a free parameter. Hierarchical clustering based on Ward's minimum variance method (numerical parameters were normalized as shown above whereas primary projecting directions were represented by one-hot encoding) was used to divide the randomly selected cells into different clusters (Figure S7E). The new entry $d(C_1, C_2)$ is computed by

$$d(C_1, C_2) = \sqrt{\frac{|C_2| + |C_3|}{T} d(C_2, C_3)^2 + \frac{|C_2| + |C_4|}{T} d(C_2, C_4)^2 - \frac{|C_2|}{T} d(C_3, C_4)^2}$$

where C_1 is the newly joined cluster consisting of cluster C_3 and C_4, C_2 is an unused cluster in the forest, and $T = C_2 + C_3 + C_4$.

Optogenetic Manipulation in Embryos

Parental flies were fed yeast paste containing 10 mM ATR for three days before collection of embryos. Both parental flies and embryos were raised in darkness before experiments. For acute optogenetic stimulation (Figure 7C), 16.5-17.5 h AEL embryos were dechorionated and placed dorsal-side-up, then 617 nm LED light at the intensity of 30 μW/mm^2 (THORLABS) was delieved for ten seconds twice at an interval of 30 seconds. For chronic optogenetic stimulation (Figure 7F), 17 h AEL embryos were placed dorsal-side-up on a fresh apple agar which was embedded in a water-filled plate to keep humidity. A 617 nm LED was connected to an eletrical stimulator (SEN-

3301; Nihon Kohden, Japan) to control the emission of light (250 μW/cm^2) periodically for two hours (for pulse duration and frequency, see Figure 7F). After stimulation, embryos were maintained in darkness and newly hatched larvae were used for the locomotion assay.

Temperature Shift Experiment

Temperature-sensitive Gal80 (TubP-Gal80^{ts}) was used for temporal knockdown of ShakB or IP_3 receptors (Figure 7E). Embryos collected in yeast-pasted agar plates were reared in incubators in which the temperature was set to 18 °C or 30 °C according to the blockade patterns (Figure 7E). Because temperature significantly alters the speed of embryonic development[85], we normalized the developmental time at 18 °C and 30 °C to that at 25 °C based on the protocol previously reported[85] and further confirmed the normalization by examining the morphology of midgut, appearance of myogenic muscle twitches and the timing of tracheal filling[3,4,85]. After applying different temporal patterns of blockades as shown in Figure 7E, newly hatched larvae were used for the locomotion assay.

QUANTIFICATION AND STATISTICAL ANALYSIS

Statistical tests were performed with Igor Pro 8, R-project and Microsoft Excel 2013 (Microsoft). Sample sizes and statistical significances are indicated in each figure panel or corresponding legend. ***$P < 0.001$, **$P < 0.01$, *$P < 0.05$, N.S., not significant and error bars indicate s.e.m. Boxplots indicate the median, 25th, 75th percentiles and whiskers above and below the box indicate the 90th and 10th percentiles respectively.

REFERENCES

1. Marder, E., and Rehm, K.J. (2005). Development of central pattern generating circuits. Curr. Opin. Neurobiol. *15*, 86–93.
2. Sanes, D.H., Reh, T.A., and Harris, W.A. (2006). Development of the Nervous System, Third Edition (Oxford: Elsevier Academic Press).
3. Crisp, S., Evers, J.F., Fiala, A., and Bate, M. (2008). The development of motor coordination in *Drosophila* embryos. Development *135*, 3707–3717.
4. Pereanu, W., Spindler, S., Im, E., Buu, N., and Hartenstein, V. (2007). The emergence of patterned movement during late embryogenesis of *Drosophila*. Dev. Neurobiol. *67*, 1669–1685.
5. O'Donovan, M.J., Chub, N., and Wenner, P. (1998). Mechanisms of spontaneous activity in developing spinal networks. J. Neurobiol. *37*, 131–145.
6. Ren, J., and Greer, J.J. (2003). Ontogeny of rhythmic motor patterns generated in the embryonic rat spinal cord. J. Neurophysiol. *89*, 1187–1195.
7. Saint-Amant, L., and Drapeau, P. (2000). Motoneuron activity patterns related to the earliest behavior of the zebrafish embryo. J. Neurosci. *20*, 3964–3972.
8. Wan, Y., Wei, Z., Looger, L.L., Koyama, M., Druckmann, S., and Keller, P.J. (2019). Single-cell reconstruction of emerging population activity in an entire developing circuit. Cell *179*, 355–372.
9. Warp, E., Agarwal, G., Wyart, C., Friedmann, D., Oldfield, C.S., Conner, A., Del Bene, F., Arrenberg, A.B., Baier, H., and Isacoff, E.Y. (2012). Emergence of patterned activity in the developing zebrafish spinal cord. Curr. Biol. *22*, 93–102.
10. Kiehn, O., and Tresch, M.C. Gap junctions and motor behavior. (2002). Trends Neurosci. *25*, 108–115.

11. Li, W.C., Roberts, A., and Soffe, S.R. (2009). Locomotor rhythm maintenance: electrical coupling among premotor excitatory interneurons in the brainstem and spinal cord of young *Xenopus* tadpoles. J. Physiol. *587*, 1677–1693.
12. Marin-Burgin, A., Eisenhart, F.J., Baca, S.M., Kristan, W.B., and French, K.A. (2005). Sequential development of electrical and chemical synaptic connections generates a specific behavioral circuit in the leech. J. Neurosci. *25*, 2478–2489.
13. Marin-Burgin, A., Kristan, W.B., and French, K.A. (2008). From synapses to behavior: Development of a sensory-motor circuit in the leech. Dev. Neurobiol. *68*, 779–787.
14. Saint-Amant, L., and Drapeau, P. (2001). Synchronization of an embryonic network of identified spinal interneurons solely by electrical coupling. Neuron *31*, 1035–1046.
15. Tresch, M.C., and Kiehn, O. (2000). Motor coordination without action potentials in the mammalian spinal cord. Nat. Neurosci. *3*, 593–599.
16. Coghill, G.E. (1929). Anatomy and the problem of behavior (London: Cambridge University Press).
17. Hamburger, V. (1963). Some aspects of the embryology of behavior. Q. Rev. Biol., *38*, 342–365.
18. Harrison, R.G. (1904). An experimental study of the relation of the nervous system to the developing musculature in the embryo of the frog. Am. J. Anat. *3*, 197–220.
19. Edwards, D.H., and Prilutsky, B.I. (2017). Sensory feedback in the control of posture and locomotion. In Neurobiology of Motor Control: Fundamental Concepts and New Directions, S.L. Hooper, A. Büschges, ed. (NJ: Wiley), pp. 263–304.
20. Pearson, K.G. (1995). Proprioceptive regulation of locomotion. Curr. Opin. Neurobiol. *5*, 786–791.
21. Blumberg, M.S., Marques, H.G., and Iida, F. (2013). Twitching in sensorimotor development from sleeping rats to robots. Curr. Biol. *23*, 532–537.
22. Llinas, R. (2002). I of the Vortex: from neurons to self (MIT Press).

23. Petersson, P., Waldenstrom, A., Fahraeus, C., and Schouenborg, J. (2003). Spontaneous muscle twitches during sleep guide spinal self-organization. Nature *424*, 72–75.

24. Ohyama, T., Schneider-Mizell, C.M., Fetter, R.D., Aleman, J.V., Franconville, R., Rivera-Alba, M., Mensh, B.D., Branson, K.M., Simpson, J.H., Truman, J.W., et al. (2015). A multilevel multimodal circuit enhances action selection in *Drosophila*. Nature *520*, 633–639.

25. Fushiki, A., Zwart, M.F., Kohsaka, H., Fetter, R.D., Cardona, A., and Nose, A. (2016). A circuit mechanism for the propagation of waves of muscle contraction in *Drosophila*. eLife *5*, e13253.

26. Kohsaka, H., Zwart, M.F., Fushiki, A., Fetter, R.D., Truman, J.W., Cardona, A., and Nose, A. (2019). Regulation of forward and backward locomotion through intersegmental feedback circuits in *Drosophila* larvae. Nat. Commun. *10*, 2654.

27. Zarin, A.A., Mark, B., Cardona, A., Litwin-Kumar, A., and Doe, C.Q. (2019). A multilayer circuit architecture for the generation of distinct locomotor behaviors in *Drosophila*. eLife *8*, e51781.

28. Zwart, M.F., Pulver, S.R., Truman, J.W., Fushiki, A., Cardona, A., and Landgraf, M. (2016). Selective inhibition mediates the sequential recruitment of motor pools. Neuron *91*, 1–14.

29. Li, H.-H., Kroll, J.R., Lennox, S.M., Ogundeyi, O., Jeter, J., Depasquale, G., and Truman, J.W. (2014). A GAL4 driver resource for developmental and behavioral studies on the larval CNS of *Drosophila*. Cell Rep. *8*, 897–908.

30. Simpson, J.H., and Looger, L.L. (2018). Functional imaging and optogenetics in *Drosophila*. Genetics *208*, 1291–1309.

31. Hughes, C.L., and Thomas, J.B. (2007). A sensory feedback circuit coordinates muscle activity in *Drosophila*. Mol. Cell. Neurosci. *35*, 383–396.

32. Song, W., Onishi, M., Jan, L.Y., and Jan, Y.N. (2007). Peripheral multidendritic sensory neurons are necessary for rhythmic locomotion behavior in Drosophila larvae. Proc. Natl. Acad. Sci. USA *104*, 5199–5204.

33. Grillner, S. (2003). The motor infrastructure: from ion channels to neuronal networks. Nature Rev. Neurosci. *4*, 573–586.

34. Marder, E., Bucher, D., Schulz, D.J., and Taylor, A.L. (2005). Invertebrate central pattern generation moves along. Curr. Biol. *15*, 685–699.

35. Pulver, S.R., Bayley, T.G., Taylor, A.L., Berni, J., Bate, M., and Hedwig, B. (2015). Imaging fictive locomotor patterns in larval *Drosophila*. J. Neurophysiol. *114*, 2564–2577.

36. Caldwell, J.C., Miller, M.M., Wing, S., Soll, D.R., and Eberl, D.F. (2003). Dynamic analysis of larval locomotion in *Drosophila* chordotonal organ mutants. Proc. Natl. Acad. Sci. USA *100*, 16053–16058.

37. Cheng, L.E., Song, W., Looger, L.L., Jan, L.Y., and Jan, Y.N. (2010). The role of the TRP channel NompC in *Drosophila* larval and adult locomotion. Neuron *67*, 373–380.

38. Guo, Y., Wang, Y., Zhang, W., Meltzer, S., Zaninig, D., Yu, Y., Li, J., Cheng, T., Guo, Z., Wang, Q., et al. (2016). Transmembrane channel-like (tmc) gene regulates *Drosophila* larval locomotion. Proc. Natl. Acad. Sci. USA *113*, 7243–7248.

39. Zlatic, M., Landgraf, M., and Bate, M. (2003). Genetic specification of axonal arbors: atonal regulates robo3 to position terminal branches in the *Drosophila* nervous system. Neuron *37*, 41–51.

40. Mogami, K., O'Donnell, P.T., Bernstein, S.I., Wright, T.R.F., and Emerson, C.P.,Jr (1986). Mutations of the *Drosophila* myosin heavy-chain gene: effects on transcription, myosin accumulation, and muscle function. Proc. Natl. Acad. Sci. USA. *83*, 1393–1397.

41. Marrus, S.B., Portman, S.L., Allen. M.J., Moffat, K.G., and DiAntonio, A. (2004). Differential localization of glutamate receptor subunits at the *Drosophila* neuromuscular junction. J. Neurosci. *24*, 1406–1415.

42. Bennett, M.V., and Zukin, R.S. (2004). Electrical coupling and neuronal synchronization in the Mammalian brain. Neuron *41*, 495–511.

43. Kandler, K., and Katz, L.C. (1995). Neuronal coupling and uncoupling in the developing nervous system. Curr. Opin. Neurobiol. *5*, 98–105.

44. Yuste, R., Peinado, A., and Katz, L.C. (1992). Neuronal domains in developing neocortex. Science *257*, 665–669.

45. Palacios-Prado, N., Huetteroth, W., and Pereda, A.E. (2014). Hemichannel composition and electrical synaptic transmission: molecular diversity and its implications for electrical rectification. Front. Cell. Neurosci. *8*, 324.

46. Pereda, A.E. (2014). Electrical synapses and their functional interactions with chemical synapses. Nat. Rev. Neurosci. *15*, 250–263.

47. Kiehn, O., and Eken, T. (1998). Functional role of plateau potentials in vertebrate motor neurons. Curr. Opin. Neurobiol. *8*, 746–752.

48. Tong, H., and McDearmid, J.R. (2012). Pacemaker and plateau potentials shape output of a developing locomotor network. Curr. Biol. *22*, 2285–2293.

49. Harris-Warrick, R.M. (2002). Voltage-sensitive ion channels in rhythmic motor systems. Curr. Opin. Neurobiol. *12*, 646–651.

50. Hille, B. (2001). Ion Channels of Excitable Membranes, Third Edition (Sinauer Associates).

51. Bading, H. (2013). Nuclear calcium signalling in the regulation of brain function. Nature Rev. Neurosci. *14*, 593–608.

52. Lytton, J., Westlin, M., and Hanley, M.R. (1991). Thapsigargin inhibits the sarcoplasmic or endoplasmic reticulum Ca-ATPase family of calcium pumps. J. Biol. Chem. *266*, 17067–17071.

53. McGuire, S.E., Mao, Z., and Davis, R.L. (2004). Spatiotemporal gene expression targeting with the TARGET and gene-switch systems in *Drosophila*. Sci. STKE *2004*, pl6.

54. Giachello, C.N., and Baines, R.A. (2015). Inappropriate neural activity during a sensitive period in embryogenesis results in persistent seizure-like behavior. Curr. Biol. *25*, 2964–2968.

55. Akay, T., Tourtellotte, W.G., Arber, S., and Jessell, T.M. (2014). Degradation of mouse locomotor pattern in the absence of proprioceptive sensory feedback. Proc. Natl. Acad. Sci. USA *111*, 16877–16882.

56. Woo, S.-H., Lukacs, V., de Nooij, J.C., Zaytseva, D., Criddle, C.R., Francisco, A., Jessell, T.M., Wilkinson, K.A., and Patapoutian, A. (2015). Piezo2 is the principal mechanotransduction channel for proprioception. Nat. Neurosci. *18*, 1756–1762.

57. Khazipov, R., Sirota, A., Leinekugel, X., Holmes, G.L., Ben-Ari, Y., and Buzsáki, G. (2004). Early motor activity drives spindle bursts in the developing somatosensory cortex. Nature *432*, 758–761.

58. Tripodi, M., Stepien, A.E., and Arber, S. (2011). Motor antagonism exposed by spatial segregation and timing of neurogenesis. Nature *479*, 61–66.

59. Suster, M.L., and Bate, M. (2002). Embryonic assembly of a central pattern generator without sensory input. Nature *416*, 174–178.

60. Park, W.-M., Wang, Y., Park, S., Denisova, J.V., Fontes, J.D., and Belousov, A.B. (2011). Interplay of chemical neurotransmitters regulates developmental increase in electrical synapses. J. Neurosci. *31*, 5909–5920.

61. Bloomfield, S.A., and Völgyi, B. (2009). The diverse functional roles and regulation of neuronal gap junctions in the retina. Nat. Rev. Neurosci. *10*, 495–506.

62. Haas, J.S., Zavala, B., and Landisman, C.E. (2011). Activity-dependent long-term depression of electrical synapses. Science *334*, 389–393.

63. Landisman, C.E., and Connors, B.W. (2005). Long-term modulation of electrical synapses in the mammalian thalamus. Science *310*, 1809–1813.

64. Welzel, G., and Schuster, S. (2018). Long-term potentiation in an innexin-based electrical synapse. Sci. Rep. *8*, 12579.

65. Spitzer, N.C. (2006). Electrical activity in early neuronal development. Nature *444*, 707–712.

66. Wenner, P. (2012). Motor development: activity matters after all. Curr. Biol. *22*, R47–R48.

67. Kandler, K., and Katz, L.C. (1998). Coordination of neuronal activity in developing visual cortex by gap junction-mediated biochemical communication. J. Neurosci. *18*, 1419–1427.

68. Nakashima, A., Ihara, N., Shigeta, M., Kiyonari, H., Ikegaya, Y., and Takeuchi, H. (2019). Structured spike series specify gene expression patterns for olfactory circuit formation. Science *365*, eaaw5030.

69. Harootunian, A.T., Kao, J.P., Paranjape, S., and Tsien, R.Y. (1991). Generation of calcium oscillations in fibroblasts by positive feedback between calcium and IP_3. Science *251*, 75–78.

70. Bezprozvanny, I., Watras, J., and Ehrlich, B.E. (1991). Bell-shaped calcium-response curves of Ins(1,4,5)P_3- and calcium-gated channels from endoplasmic reticulum of cerebellum. Nature *351*, 751–754.

71. Blankenship, A., and Feller, M. (2010). Mechanisms underlying spontaneous patterned activity in developing neural circuits. Nat. Rev. Neurosci. *11*, 18–29.

72. Antón-Bolaños, N., Sempere-Ferràndez, A., Guillamón-Vivancos, T., Martini, F.J., Pérez-Saiz, L., Gezelius, H., Filipchuk, A., Valdeolmillos, M., and López-Bendito, G. (2019). Prenatal activity from thalamic neurons governs the emergence of functional cortical maps in mice. Science *364*, 987–990.

73. Katz, L.C., and Shatz, C.J. (1996). Synaptic activity and the construction of cortical circuits. Science *274*, 1133–1138.

74. Thompson, A., Gribizis, A., Chen, C., and Crair, M.C. (2017). Activity-dependent development of visual receptive fields. Curr. Opin. Neurobiol. *42*, 136–143.

75. Ackman, J.B., Burbridge, T. J., and Crair, M. C. (2012). Retinal waves coordinate patterned activity throughout the developing visual system. Nature *490*, 219–225.

76. Hubel, D.H., and Wiesel, T.N. (1970). The period of susceptibility to the physiological effects of unilateral eye closure in kittens. J. Physiol. *206*, 419–436.

77. Meister, M., Wong, R.O., Baylor, D.A., and Shatz, C.J. (1991). Synchronous bursts of action potentials in ganglion cells of the developing mammalian retina. Science *252*, 939–943.

78. Stellwagen, D., and Shatz, C.J. (2002). An instructive role for retinal waves in the development of retinogeniculate connectivity. Neuron *33*, 357–367.

79. Moreno-Juan, V., Filipchuk, A., Antón-Bolaños, N., Mezzera, C., Gezelius, H., Andrés, B., Rodríguez-Malmierca, L., Susín, R., Schaad, O., Iwasato, T., et al. (2017). Prenatal thalamic waves regulate cortical area size prior to sensory processing. Nat. Commun. *8*, 14172.

80. Frangeul, L., Kehayas, V., Sanchez-Mut, J.V., Fièvre, S., Krishna-K, K., Pouchelon, G., Telley, L., Bellone, C., Holtmaat, A., Gräff, J., et al. (2017). Input-dependent regulation of excitability controls dendritic maturation in somatosensory thalamocortical neurons. Nat. Commun. *8*, 2015.

81. Lin, D.M., and Goodman, C.S. (1994). Ectopic and increased expression of Fasciclin II alters motoneuron growth cone guidance. Neuron *13*, 507–523.

82. Marley, R., and Baines, R.A. (2011). Dissection of first- and second-instar *Drosophila* larvae for electrophysiological recording from neurons: the flat (or fillet) preparation. Cold Spring Harb. Protoc. *2011*, 2011.

83. Choi, J.C., Park, D., and Griffith, L.C. (2004). Electrophysiological and morphological characterization of identified motor neurons in the *Drosophila* third instar larva central nervous system. J. Neurophysiol. *91*, 2353–2365.

84. Inada, K., Tsuchimoto, Y., and Kazama, H. (2017). Origins of cell-type-specific olfactory processing in the *Drosophila* mushroom body circuit. Neuron *95*, 357–367.

85. Chong, J., Amourda, C., and Saunders, T.E. (2018). Temporal development of *Drosophila* embryos is highly robust across a wide temperature range. J. R. Soc. Interface *15*, 20180304.

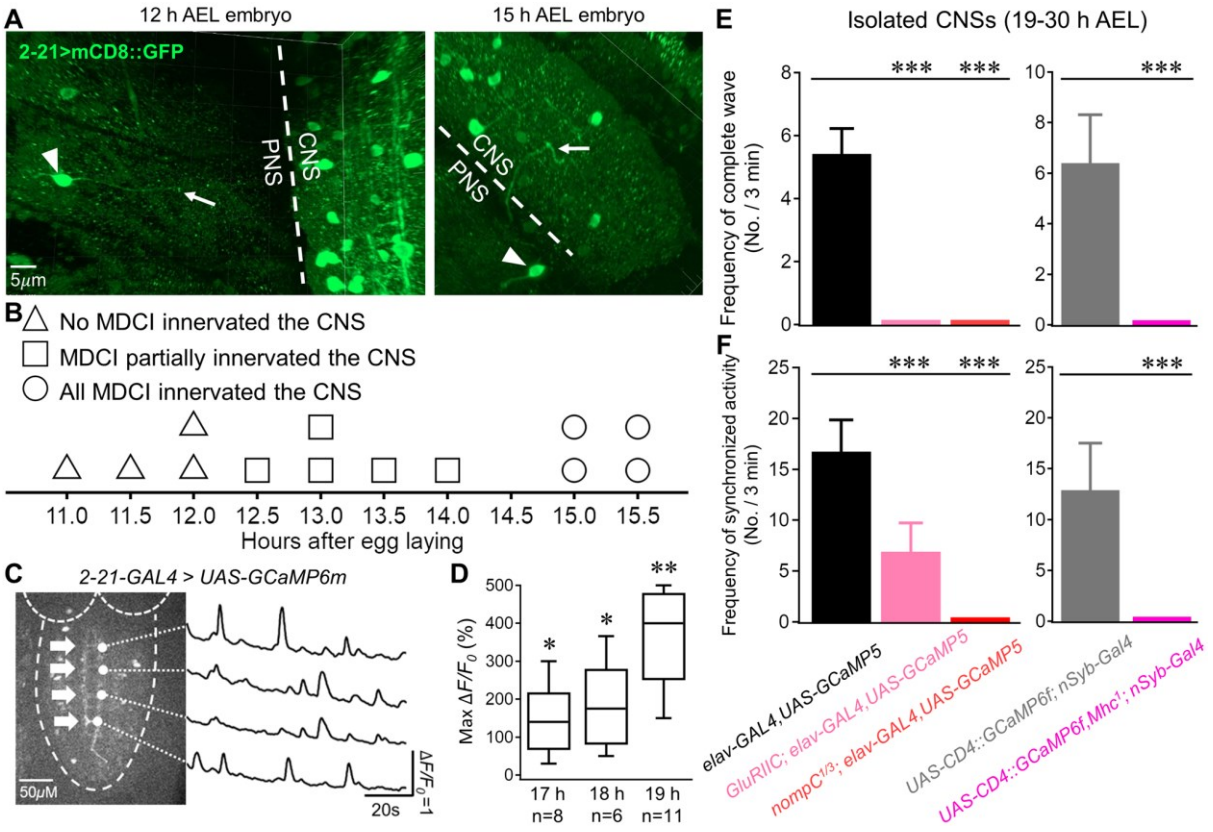

Figure S1. Development of proprioceptive class I da neurons and CPG defects in mutants lacking proprioception, related to Figure 1

(A) Axon projection of a class I da neuron (vpda) at 12 (left) and 15 h (right) AEL. Arrowheads and arrows denote the somata and axon terminals respectively. Dashed lines indicate the border between the CNS and PNS.

(B) Timeline summary of central innervation of class I da neurons. Each symbol represents an individual embryo. Note that class I da neurons fully innervated the CNS by ~15 h AEL. Bipolar dendrite and chordotonal neurons also innervate the CNS prior to the emergence of motor activities[39].

(C) An example of calcium imaging from axonal terminals of class I da neurons at ~18 h AEL. Arrows denote the axon terminals in the left hemi-segments and ROIs (filled circles) were set on the terminals of the right hemisegments.

(D) Quantification of the calcium signals (normalized by the baselines) at different embryonic stages. Mann–Whitney U test followed by Holm–Bonferroni correction. Boxplots indicate the

median, 25th, 75th percentiles and whiskers above and below the box indicate the 90th and 10th percentiles respectively, in this and the following figures.

(E and F) Quantification of complete waves (E) and sychronized activities (F) in controls and mutants with impaired proprioception (19-30 h AEL embryos/larvae). n = 39, 26, 54, 19, 14 from left to right. Mann–Whitney U test followed by Holm–Bonferroni correction.

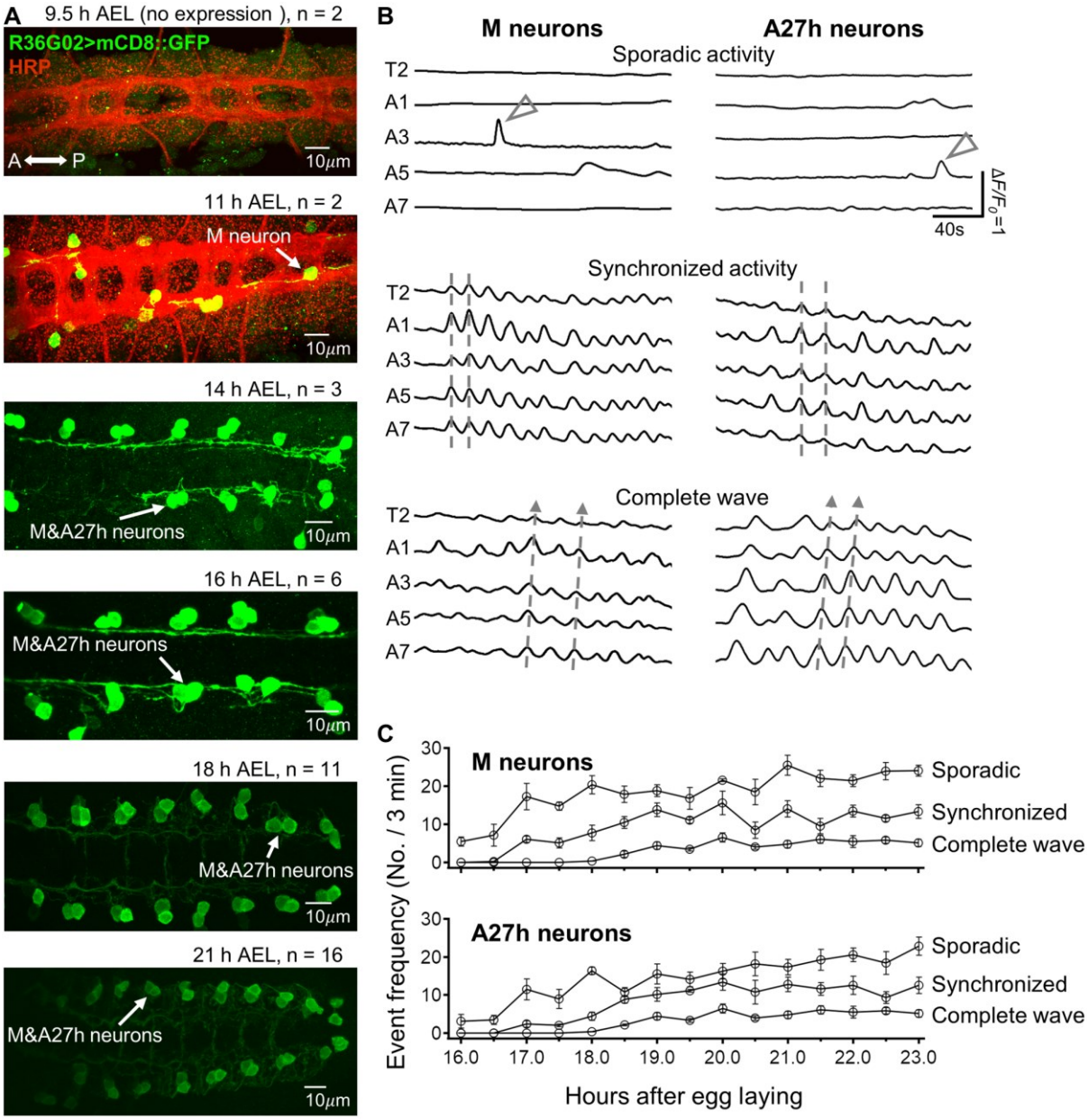

Figure S2. Emergence of patterned activity in M and A27h neurons, related to Figure 2

(A) Typical confocal images obtained from *R36G02-Gal4* > *UAS-mCD8::GFP* embryos at various embryonic stages. Note that expression is seen in M and A27h neurons from 11 h and 14 h AEL respectiely. At early stages, horseradish peroxidase (HRP) staining was used to label the commissures. The Gal4-driven expression is largely restricted to M and A27h neurons with the exception of expression in a few brain cells.

(B) Representative examples of each activity pattern observed in M neurons (left) and A27h neurons (right). Note that synchronized activities shown here are among the same cell types.

(C) Plots of event frequencies of each activity pattern against developmental stages. n ≥ 2 embryos at each stage.

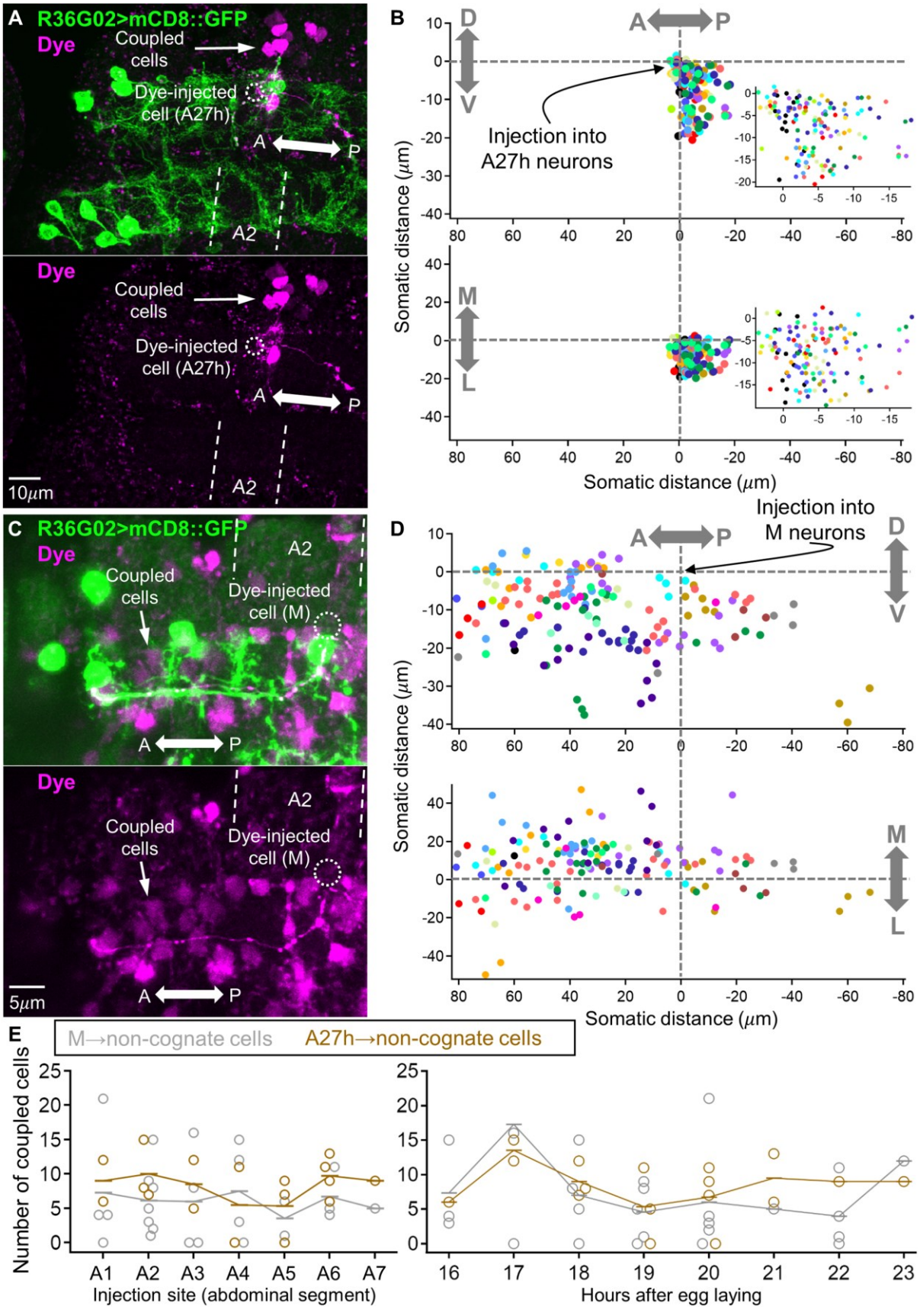
A
R36G02>mCD8::GFP
Dye
Coupled cells
Dye-injected cell (A27h)
A
P
A2
Dye
Coupled cells
Dye-injected cell (A27h)
A
P
A2
10μm
B
D
V
A
P
Injection into A27h neurons
Somatic distance (μm)
M
L
Somatic distance (μm)
C
R36G02>mCD8::GFP
Dye
A2
Coupled cells
Dye-injected cell (M)
A
P
Dye
A2
Coupled cells
Dye-injected cell (M)
A
P
5μm
D
Injection into M neurons
A
P
D
V
Somatic distance (μm)
M
L
Somatic distance (μm)
E
M→non-cognate cells
A27h→non-cognate cells
Number of coupled cells
A1
A2
A3
A4
A5
A6
A7
Injection site (abdominal segment)
16
17
18
19
20
21
22
23
Hours after egg laying

Figure S3. Coupling of M and A27h neurons to other interneurons in the nerve cord, related to Figure 2

(A) An example of coupling following injection into an A27h neuron.

(B) Plots of somatic distances from injected cells (A27h) to coupled cells. A, anterior; P, posterior; D, dorsal; V, ventral; L, lateral; M, medial. Cells coupled with the same A27h neuron are plotted in the same color (n = 17 A27h neurons). Insets show expanded view.

(C and D) The same as (A) and (B) but for M neurons (n = 25 M neurons). Consistent with the short and long A-P projection of A27h and M axons (Figures 2B–2E), coupled cells were clustered and spread across segments for A27h and M neurons, respectively.

(E) Plots of number of coupled cells against injection sites (left) and developmental stages (right). Unlike cognate coupling, non-cognate couplings are not segment-specific. Note also that the number of coupled cells did not show dramatic changes during development.

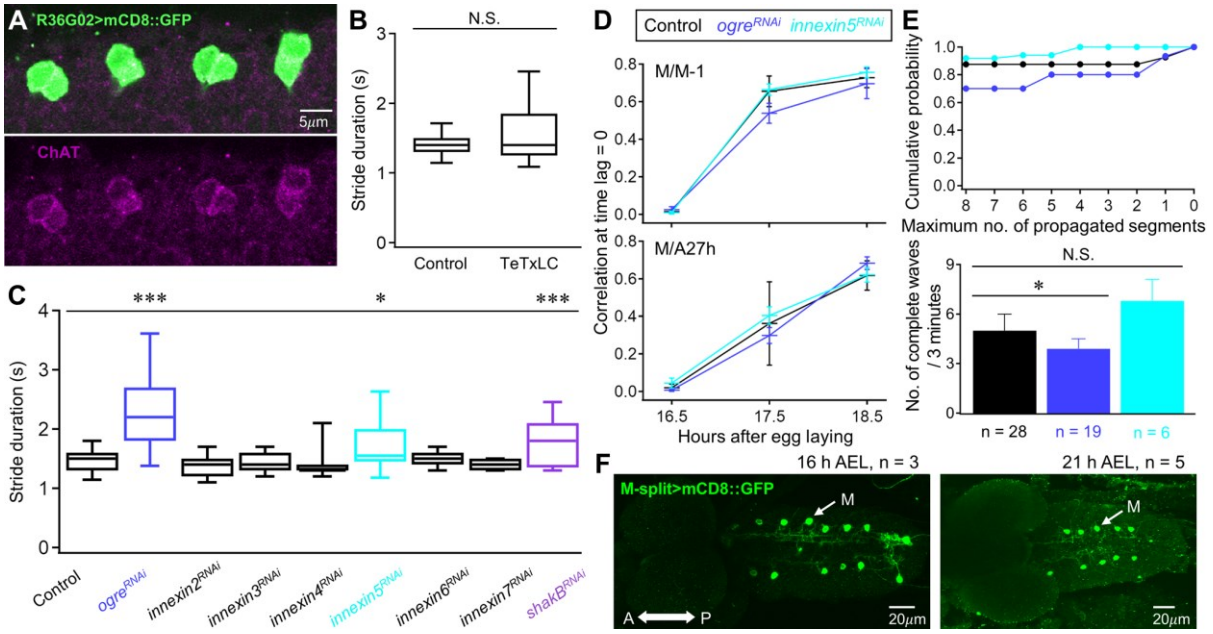

Figure S4. Electrical but not chemical transmission in M/A27h circuits is important for motor development, related to Figure 3

(A) Somata of M and A27h neurons are immunoreactive to ChAT.

(B) Quantification of stride duration in newly hatched control (*UAS-TeTxLC/+*) and *R36G02-Gal4 > UAS-TeTxLC* larvae. n = 20 larvae for both groups. Two-tailed Student's t-test.

(C) Effects of RNAi knockdown of innexin genes in M and A27h neurons on stride duration of locomotion (newly hatched larvae). All the eight innexin genes present in the *Drosophila* genome were examined. n > 10 larvae for each group. Expression of each RNAi construct was driven by *R36G02-Gal4* and thus *R36G02-Gal4/+* larvae were used as a control. Two-tailed Student's t-test followed by Holm–Bonferroni correction.

(D) The same as in Figure 3A, but for *ogre*^{RNAi} (n = 7, 4, 5 for embryos at 16.5, 17.5 and 18.5 h AEL) and *innexin5*^{RNAi} (n = 4, 6, 5). Synchronized activities in the M/A27h circuits are normal in *R36G02-Gal4 > UAS-ogre*^{RNAi} and *R36G02-Gal4 > UAS-innexin5*^{RNAi}. *P* > 0.05 comparing between genotypes, two-way ANOVA followed by Tukey's *post hoc* analysis.

(E) The same as in Figure 3B, but for *ogre*^{RNAi} and *innexin5*^{RNAi}. Only mild abnormalities were seen in fictive waves in the *R36G02-Gal4 > UAS-ogre*^{RNAi} embryos/larvae (19-30 h AEL).

Mann–Whitney U test followed by Holm–Bonferroni correction.

(F) Typical confocal images obtained from *M-split-Gal4* > *UAS-mCD8::GFP* embryos at 16 and 21 h AEL respectively.

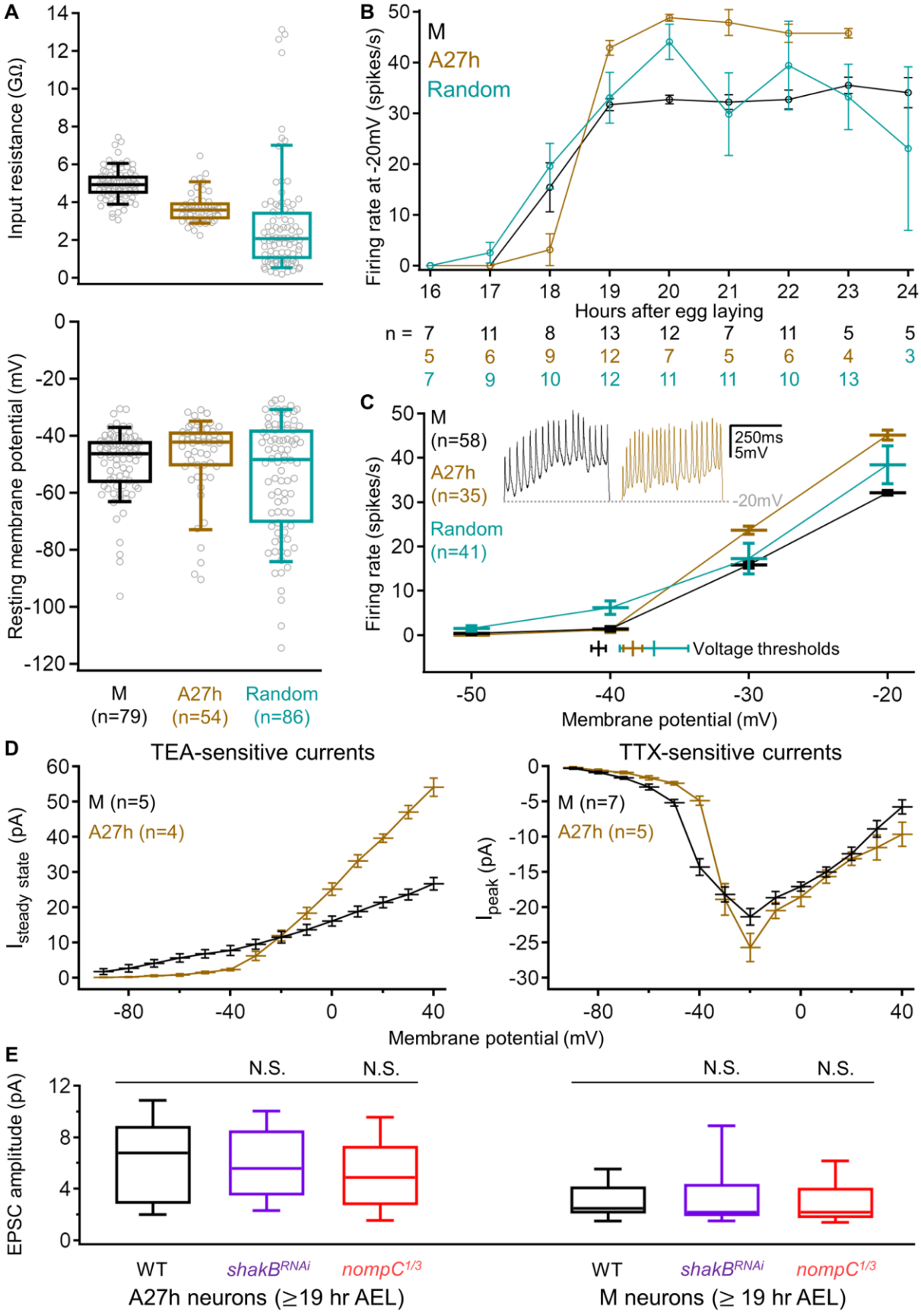
A
Input resistance (GΩ)
Resting membrane potential (mV)
M (n=79)
A27h (n=54)
Random (n=86)
B
M
A27h
Random
Firing rate at -20mV (spikes/s)
Hours after egg laying
n = 7 11 8 13 12 7 11 5 5
5 6 9 12 7 5 6 4 3
7 9 10 12 11 11 10 13
C
M (n=58)
A27h (n=35)
Random (n=41)
250ms
5mV
-20mV
Voltage thresholds
Firing rate (spikes/s)
Membrane potential (mV)
D
TEA-sensitive currents
M (n=5)
A27h (n=4)
I steady state (pA)
TTX-sensitive currents
M (n=7)
A27h (n=5)
I peak (pA)
Membrane potential (mV)
E
N.S.
N.S.
N.S.
N.S.
EPSC amplitude (pA)
WT
shakB RNAi
nompC 1/3
A27h neurons (≥19 hr AEL)
M neurons (≥ 19 hr AEL)

Figure S5. Electrophysiological properties of M and A27h neurons, related to Figure 5

(A) Plots of the input resistance (top) and resting membrane potential (bottom) in M, A27h and randomly selected cells (Random) in the nerve cord.

(B) Plot of the firing rate at -20mV against developmental stages. Action potentials can be evoked reliably from ~19 h AEL in M and A27h neurons.

(C) Plot of the firing rate against the membrane potential (voltage threshold for each cell type are also shown at the bottom). Only cells capable of firing action potentials were used for the analyses.

(D) Current-voltage curves for tetraethylammonium (TEA)-sensitive steady-state currents (left) and TTX-sensitive peak currents (right). 50 mM TEA and 1 μM TTX were bath-applied to block potassium (including both voltage-gated and Ca^{2+}-activated K^+ currents) and voltage-gated sodium currents, respectively. Currents were isolated by subtracting the traces from those recorded in saline.

(E) Quantification of EPSC amplitude in each genotype. n = 34, 18, 24, 53, 9, 32 cells from left to right (19-24 h AEL embryos/larvae). Neurons were voltage-clamped at -60 mV. Mann–Whitney U test followed by Holm–Bonferroni correction.

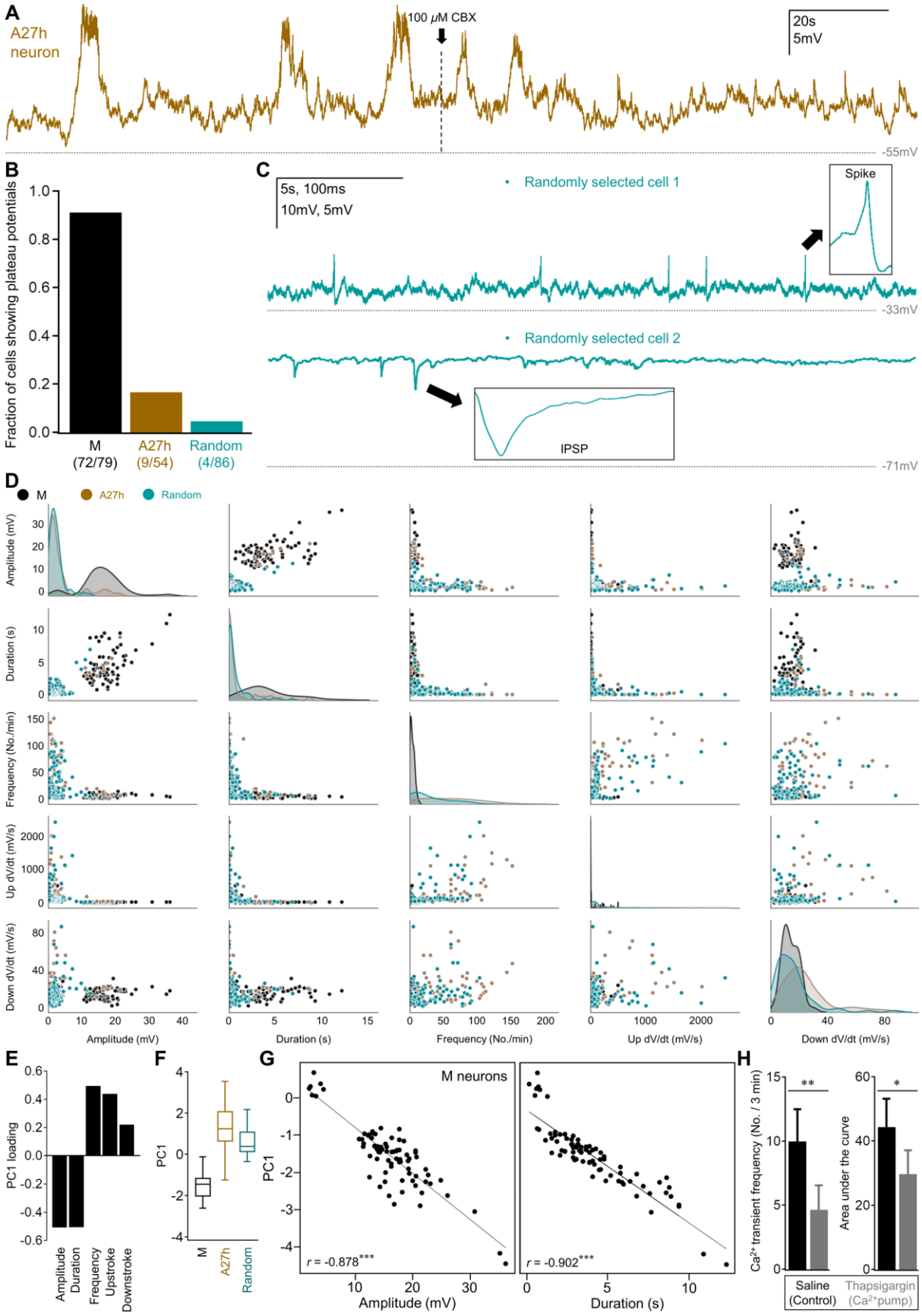
A
A27h neuron
100 μM CBX
20s
5mV
-55mV
B
Fraction of cells showing plateau potentials
1.0
0.8
0.6
0.4
0.2
0.0
M (72/79)
A27h (9/54)
Random (4/86)
C
5s, 100ms
10mV, 5mV
Randomly selected cell 1
Spike
-33mV
Randomly selected cell 2
IPSP
-71mV
D
M
A27h
Random
Amplitude (mV)
Duration (s)
Frequency (No./min)
Up dV/dt (mV/s)
Down dV/dt (mV/s)
E
PC1 loading
Amplitude
Duration
Frequency
Upstroke
Downstroke
F
PC1
M
A27h
Random
G
M neurons
PC1
r = -0.878***
Amplitude (mV)
r = -0.902***
Duration (s)
H
Ca2+ transient frequency (No. / 3 min)
**
Area under the curve
*
Saline (Control)
Thapsigargin (Ca2+pump)

Figure S6. Plateau potential is uniquely generated by M neurons, related to Figure 6

(A) An example of plateau potentials generated in an A27h neuron, which were abolished after addition of 100 μM CBX.

(B) Fraction of cells that generated plateau potentials.

(C) Example traces from three randomly selected cells that showed spontaneous firing (top), IPSPs (middle) and EPSPs (bottom). Plateau potentials are not present.

(D) Plots of the spontaneous activity amplitude, steady-state duration, frequency, kinetics of upstroke and downstroke of M, A27h and randomly selected cells (n = 79, 54, 86 respectively). Diagonal axes represent the univariate distribution of the data for the variable in that column. Except for 4 out of 86 randomly selected cells showing plateau potentials (B), the remaining 82 cells only exhibited occasional short-lasting events such as excitatory and/or inhibitory PSPs, and spontaneous firing (C). These characteristics were used for PCA and classification as shown in Figure 6E.

(E) PC1 loadings on each of the five dimensions.

(F) Plot of mean PC1 scores of each cell type.

(G) Plots of PC1 scores against the amplitude (left) and the steady-state duration (right) for M neurons. Note that the amplitude and the duration are significantly correlated with PC1.

(H) Quantifications of frequency (left) and avearage area under the curve (right) of M neurons' calcium transients in control (saline) and 1 μM thapsigargin. 16-17 h AEL *R36G02-Gal4* > *UAS-GCaMP6m* embryos were used. n = 8 and 12 embryos in saline and thapsigargin respectively. Mann–Whitney U test.

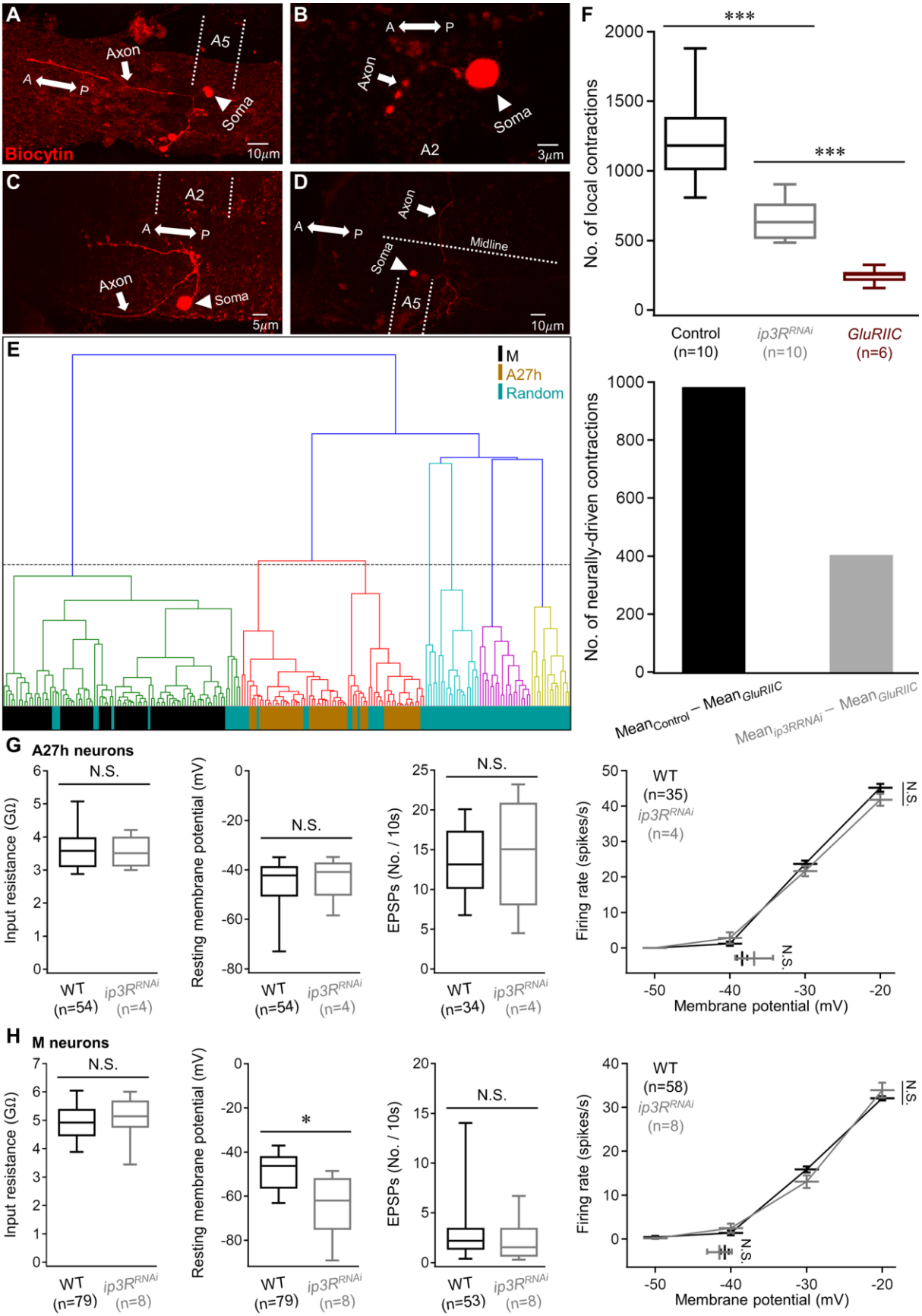
A
Axon
A5
A
P
Soma
Biocytin
10μm
B
A
P
Axon
Soma
A2
3μm
C
A2
A
P
Axon
Soma
5μm
D
A
P
Axon
Midline
Soma
A5
10μm
E
M
A27h
Random
F
***
***
No. of local contractions
2000
1500
1000
500
0
Control
(n=10)
ip3R^RNAi
(n=10)
GluRIIC
(n=6)
No. of neurally-driven contractions
1000
800
600
400
200
0
Mean_Control – Mean_GluRIIC
Mean_ip3RRNAi – Mean_GluRIIC
G
A27h neurons
Input resistance (GΩ)
N.S.
WT
(n=54)
ip3R^RNAi
(n=4)
Resting membrane potential (mV)
N.S.
WT
(n=54)
ip3R^RNAi
(n=4)
EPSPs (No. / 10s)
N.S.
WT
(n=34)
ip3R^RNAi
(n=4)
Firing rate (spikes/s)
WT
(n=35)
ip3R^RNAi
(n=4)
N.S.
N.S.
Membrane potential (mV)
H
M neurons
Input resistance (GΩ)
N.S.
WT
(n=79)
ip3R^RNAi
(n=8)
Resting membrane potential (mV)
*
WT
(n=79)
ip3R^RNAi
(n=8)
EPSPs (No. / 10s)
N.S.
WT
(n=53)
ip3R^RNAi
(n=8)
Firing rate (spikes/s)
WT
(n=58)
ip3R^RNAi
(n=8)
N.S.
N.S.
Membrane potential (mV)

Figure S7. A Variety of cell types are included in randomly selected cells and behavioral/physiological impacts of knockdown of IP_3 receptors in M and A27h neurons, related to Figures 6 and 7

(A–D) Various anatomies of randomly selected cells, visualized by biocytin injection. (A) an ascending neuron (17.5 h AEL). (B) a local neuron (18 h AEL). (C) a motor neuron (22 h AEL). (D) a contralaterally projecting neuron (23 h AEL).

(E) Dendrogram of hierarchical clustering of patch-clamp recoding datasets. Clustering was based on the input resistance, resting membrane potential, firing rate at -20 mV, steady-state current, axonal length and primary projecting direction (dorsal, ventral, anterior, posterior, medial or lateral). Each column corresponds to an individual cell. Based on the distance that seperates M and A27h neurons (horizontal dashed line), at least six cell types were included in randomly selected cells.

(F) Quantification of the number of total local contractions in control (*UAS-ip3R*^{RNAi}/+), IP_3R-knockdown (*R36G02-GAL4 > UAS-ip3R*^{RNAi}) and *GluRIIC* mutants (top). Mann–Whitney U test followed by Holm–Bonferroni correction. Average number of muscle-autonomous contractions seen in *GluRIIC* was subtracted from the total number of contractions seen in control and IP_3R-knockdown embryos to obtain “estimated” number of neurally-driven contractions (bottom) and normalized to the level of control (Figure 7B).

(G and H) Quantification of the input resistance, resting membrane potential, EPSP frequency, firing rate and threshold of A27h (G) and M neurons (H). Note that these physiological properties are normal in IP_3R-knockdown A27h neurons and only the resting membrane potential was affected in IP_3R-knockdown M neurons. Mann–Whitney U test (except for comparison of firing rate, two-way ANOVA). 19-24 h AEL embryos/larvae were used for the analyses of EPSP frequency and only cells capable of firing action potentials were used for the analyses of firing rate.